Eocene Terrane Accretion in Northern Cascadia Recorded by Brittle Left-Lateral Slip on the San Juan Fault

Nicolas Harrichhausen, Kristin D. Morell, Christine Regalla, Emerson M. Lynch, Lucinda J. Leonard

May 2022

Tectonics®

RESEARCH ARTICLE
10.1029/2022TC007317

Key Points:

- The San Juan fault is a high-angle fault that accommodated brittle left-lateral slip
- Cross-cutting relations between the fault, metamorphic foliation, and overlying sediments, constrain left lateral slip to the Eocene
- Eocene left-lateral slip is consistent with strain induced by the accretion of the Siletzia terrane

Supporting Information:

Supporting Information may be found in the online version of this article.

Correspondence to:

N. Harrichhausen,
n.harrichhausen@univ-grenoble-alpes.fr

Citation:

Harrichhausen, N., Morell, K. D., Regalla, C., Lynch, E. M., & Leonard, L. J. (2022). Eocene terrane accretion in northern Cascadia recorded by brittle left-lateral slip on the San Juan fault. *Tectonics*, *41*, e2022TC007317. https://doi.org/10.1029/2022TC007317

Received 21 MAR 2022
Accepted 4 OCT 2022

Author Contributions:

Conceptualization: Nicolas Harrichhausen, Kristin D. Morell, Christine Regalla
Formal analysis: Nicolas Harrichhausen
Funding acquisition: Nicolas Harrichhausen, Kristin D. Morell, Christine Regalla
Investigation: Nicolas Harrichhausen, Kristin D. Morell, Christine Regalla, Emerson M. Lynch, Lucinda J. Leonard
Project Administration: Kristin D. Morell, Christine Regalla
Supervision: Kristin D. Morell
Visualization: Nicolas Harrichhausen
Writing – original draft: Nicolas Harrichhausen

Eocene Terrane Accretion in Northern Cascadia Recorded by Brittle Left-Lateral Slip on the San Juan Fault

Nicolas Harrichhausen[1,2], Kristin D. Morell[1], Christine Regalla[3], Emerson M. Lynch[3], and Lucinda J. Leonard[4]

[1]Department of Earth Science, University of California, Santa Barbara, CA, USA, [2]Now at Univ. Grenoble Alpes, Univ. Savoie Mont Blanc, CNRS, IRD, Univ. Gustave Eiffel, ISTerre, Grenoble, France, [3]School of Earth and Sustainability, Northern Arizona University, Flagstaff, AZ, USA, [4]School of Earth and Ocean Sciences, University of Victoria, Victoria, BC, Canada

Abstract The San Juan fault (SJF), on southern Vancouver Island, Canada, juxtaposes the oceanic Wrangellia and Pacific Rim terranes in the northern Cascadia forearc, and has been suggested to play a role in multiple Mesozoic-Cenozoic terrane accretion events. However, direct observations of the SJF's kinematics have not been documented and its exact role in accommodating strain arising from terrane accretion is unknown. To test if, how, and when the SJF accommodated accretion-related strain, we use geologic mapping, kinematic inversion of fault-plane slickenlines, and dating of marine sediments to constrain the timing and direction of brittle slip of the SJF. *P*- and *T*-axes from kinematic inversions indicate predominantly left-lateral slip. Left-lateral brittle faulting cross-cuts ~51 Ma magmatic intrusions and foliation, providing a maximum age of brittle deformation. The fault zone is non-conformably overlain by a >300 m-thick sequence of clastic marine shelf and slope sediments that are not left-laterally offset. A strontium isotope age of foraminifers helps constrain the depositional age of the sediments to late Eocene–early Oligocene, bracketing left-lateral slip to the Eocene. Eocene left-lateral slip is temporally and kinematically consistent with regional southwest-northeast compression during accretion of the Siletzia ocean island plateau, suggesting brittle slip on the SJF accommodated strain resulting from the accretion of this terrane. This result does not support hypotheses that brittle slip along the SJF directly accommodated earlier accretion of the Pacific Rim terrane to Wrangellia, instead it offsets the older accretionary boundary between these two terranes.

1. Introduction

The subduction of oceanic plateaus, seamounts, and island arcs at convergent margins can cause the accretion of lower-plate material to the upper plate, often resulting in significant permanent forearc deformation (e.g., Brandon et al., 1998; Clowes et al., 1987; Hasebe & Tagami, 2001; Menant et al., 2020; Parsons et al., 1999). Northern Cascadia, along the western margin of North America, presents a classic example of accretion of oceanic terranes. Sequential accretion of the Intermontane belt, Wrangellia, and Siletzia, along with smaller associated terranes has shaped the geology of the western ~1,000 km of the North American continental crust throughout the Mesozoic and Cenozoic (e.g., Davis et al., n.d; Dickinson, 2004; Monger et al., 1982; Wells et al., 1984). The latest of these events, the Eocene accretion of Siletzia, is considered a prime example of a large Iceland-like ocean island plateau colliding with the upper plate (e.g., Eddy et al., 2017; Kant et al., 2018; Massey, 1986; Miller et al., 2022; Wells et al., 1984), however the strain record resulting from this collision remains incompletely understood.

On southern Vancouver Island, Canada, several major tens to hundreds kilometers long terrane-juxtaposing faults (the San Juan, Survey Mountain, and Leech River faults) separate the westernmost basement terranes that were involved in the latest accretion event (Wrangellia, Pacific Rim terrane, and Siletzia; e.g., Fairchild & Cowan, 1982; Monger, 1977; Wells et al., 2014, 1984). These faults have been considered to play a significant and primary role in the addition of lower plate material to the crust of the upper plate, and to have accommodated large displacements resulting from accretion (e.g., Brandon, 1989b; Fairchild & Cowan, 1982; Groome et al., 2003; Johnson, 1984a). However, exactly how the terrane-juxtaposing faults in northern Cascadia accommodated accretion, and whether the deformation associated with the accretion events mainly occurs across a single structure, or is distributed across a network of structures, remain ambiguous (England & Calon, 1991; Fairchild & Cowan, 1982; Johnson, 1984a; Rusmore & Cowan, 1985).

Writing – review & editing: Kristin D. Morell, Christine Regalla, Emerson M. Lynch, Lucinda J. Leonard

Located in the Cascadia forearc of southern Vancouver Island, the San Juan fault (SJF) places the southern extent of the Wrangellia terrane in fault contact with accretionary prism and melange rocks of the Pacific Rim terrane (Figure 1). Although this major terrane-juxtaposing structure is documented to play a pivotal role in the amalgamation of the northern Cascadia forearc (Figure 1; England & Calon, 1991; Johnson, 1984a; Muller, 1977; Rusmore & Cowan, 1985), there are several competing hypotheses regarding its role in forearc deformation and terrane accretion. This structure is traditionally considered as a thrust fault that accommodated the accretion of the Pacific Rim terrane to the upper plate in the late Cretaceous to early Eocene (Brandon, 1989b; MacLeod et al., 1977; Muller, 1977). However, it is suggested that the SJF could have instead facilitated significant Mesozoic forearc translation via strike-slip faulting (Johnson, 1984a; Rusmore & Cowan, 1985), while others speculate it was a tear fault related to the Eocene accretion of the oceanic plateau of the Siletzia terrane (Figure 1, England & Calon, 1991; Fairchild & Cowan, 1982).

In this article, we place new constraints on the timing and slip history of the SJF using geologic mapping, fault kinematics from fault plane slickenlines, and new stratigraphic ages from strontium (Sr) isotope dating of foraminifers in marine sedimentary rocks. These analyses, together with cross-cutting relationships between previously dated metamorphic foliation and igneous intrusions, bracket the timing of brittle slip on the SJF and its associated kinematics. Our results challenge the hypotheses that the brittle SJF was primarily a reverse structure or right-lateral fault formed in response to the accretion of the Pacific Rim terrane. Instead, we suggest that it was a major brittle left-lateral fault that accommodated forearc deformation in response to the Eocene accretion of the Siletzia terrane, and that it cross-cuts the older terrane-bounding structure between Wrangellia and the Pacific Rim terrane.

2. Mesozoic-Cenozoic Terrane Accretion on Southern Vancouver Island

The assembly, deformation, and sedimentation history of the northern Cascadia forearc have been greatly affected by the accretion of geologic terranes to ancestral North America throughout the late Mesozoic to Cenozoic eras. Three of these major accreted terranes, Wrangellia, Pacific Rim, and Siletzia, have been mapped on southern Vancouver Island (Figure 1; MacLeod et al., 1977; Muller, 1977; Rusmore & Cowan, 1985).

The island arc and oceanic plateau related rocks of Wrangellia, which lie north of the SJF (Figure 1), were accreted to North America during the Mesozoic (e.g., Brandon et al., 1986; Monger, 1977; Monger et al., 1982; Sigloch & Mihalynuk, 2017). Wrangellian basement consists of Paleozoic island arc-related volcanic and sedimentary rocks, overlain by a sequence of Triassic ocean island basalts and marine sediments (Figure 2, Brandon et al., 1986; Monger, 1977; Monger & Journeay, 1994). The Cretaceous forearc basin sediments of the Nanaimo Group were deposited atop Wrangellian basement following accretion (England & Calon, 1991; Mustard 1994; Mustard et al., 1995), followed by the deposition of Paleocene to Middle Eocene fluvial sediments of the Chuckanut Formation in Washington State (Johnson, 1984b; Mustoe et al., 2007).

The Pacific Rim terrane, south of the SJF (Figure 1), is suggested to have accreted to or been juxtaposed against ancestral North America along the SJF and/or Survey Mountain faults (Figure 2; Brandon, 1989b; Fairchild & Cowan, 1982; Groome et al., 2003; Rusmore & Cowan, 1985). The terrane is composed of Jurassic to Paleocene pelagic and shelf sediments, and volcanics that accreted to the upper plate during the Late Cretaceous to Eocene (Fairchild & Cowan, 1982; Rusmore & Cowan, 1985). Two separate units, the Pandora Peak unit and Leech River Complex, have been mapped within the Pacific Rim terrane (Figure 2). The Pandora Peak unit is interpreted as a subduction zone melange, consisting of interbedded lawsonite-bearing argillite and greywacke, and tectonic blocks of tuff, chert, and minor limestone. The Pandora Peak unit underwent high-P, low-T metamorphism in the Late Cretaceous between 99 and 83 Ma (Rusmore & Cowan, 1985), and contains a metamorphic assemblage distinct from Wrangellia (Brandon, 1989b; MacLeod et al., 1977; Muller, 1977). The Leech River Complex is south of the Pandora Peak unit and is composed primarily of pelitic rocks (Figure 2), which underwent high-T, low-P, greenschist-to amphibolite-grade metamorphism at 51 Ma (Groome et al., 2003), or between 41 and 39 Ma (Fairchild & Cowan, 1982). The nature of the contact between the Pandora Peak and Leech River Complex is not known, but their distinct metamorphic histories suggest they may be in fault contact (Rusmore & Cowan, 1985).

Eocene accretion of the Siletzia ocean island plateau basalts to northern Cascadia resulted in extensive and widespread deformation across the ancient forearc (e.g., Eddy et al., 2016; England & Calon, 1991; Groome et al., 2003; Johnston & Acton, 2003; Miller et al., 2016; Wells et al., 2014). Previous studies suggest that

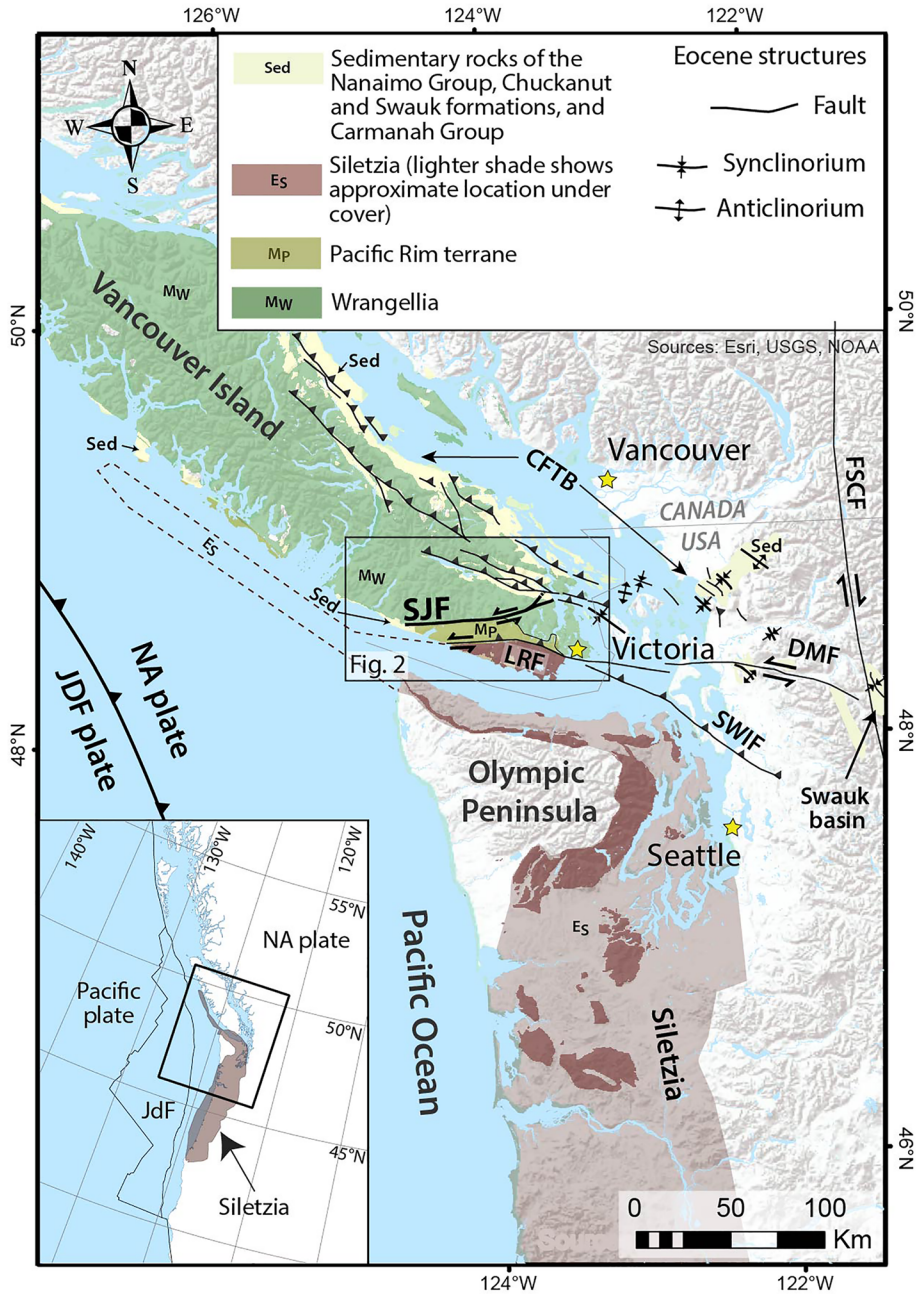

Figure 1. Geologic terrane map of northern Cascadia showing the San Juan fault (SJF) and related structures that may have resulted from terrane accretion. The implied fault slip and shortening during the accretion of Siletzia is shown on the Leech River fault (LRF), South Whidbey Island fault (SWIF), Devils Mountain fault (DMF), the Cowichan fold and thrust belt (CFTB), the Swauk basin, and the Fraser–Straight Creek fault (FSCF). The modern subduction zone where the Juan de Fuca (JDF) plate subducts beneath the North America (NA) plate is shown for reference. Light brown shows location of Siletz terrane under cover. Inset shows full extent of Siletzia on the western margin of North America, and the extent of the main figure (black box). Adapted from Bird (2003), Cui et al. (2017), Miller et al. (2016), Phillips et al. (2017), and Schuster (2005).

Siletzia accretion occurred along the South Whidbey Island and Leech River fault zones, causing Siletzia to be placed in fault contact with the Leech River Complex of the Pacific Rim terrane (Figure 2, Calvert, 1996; Clowes et al., 1987; Hyndman et al., 1990; Sherrod et al., 2008). Siletzia accretion has also been associated with crustal shortening in the inner forearc. For example, the Cowichan fold and thrust belt is documented to have accommodated extensive southwest-northeast crustal shortening among the sediments of the Nanaimo Group and

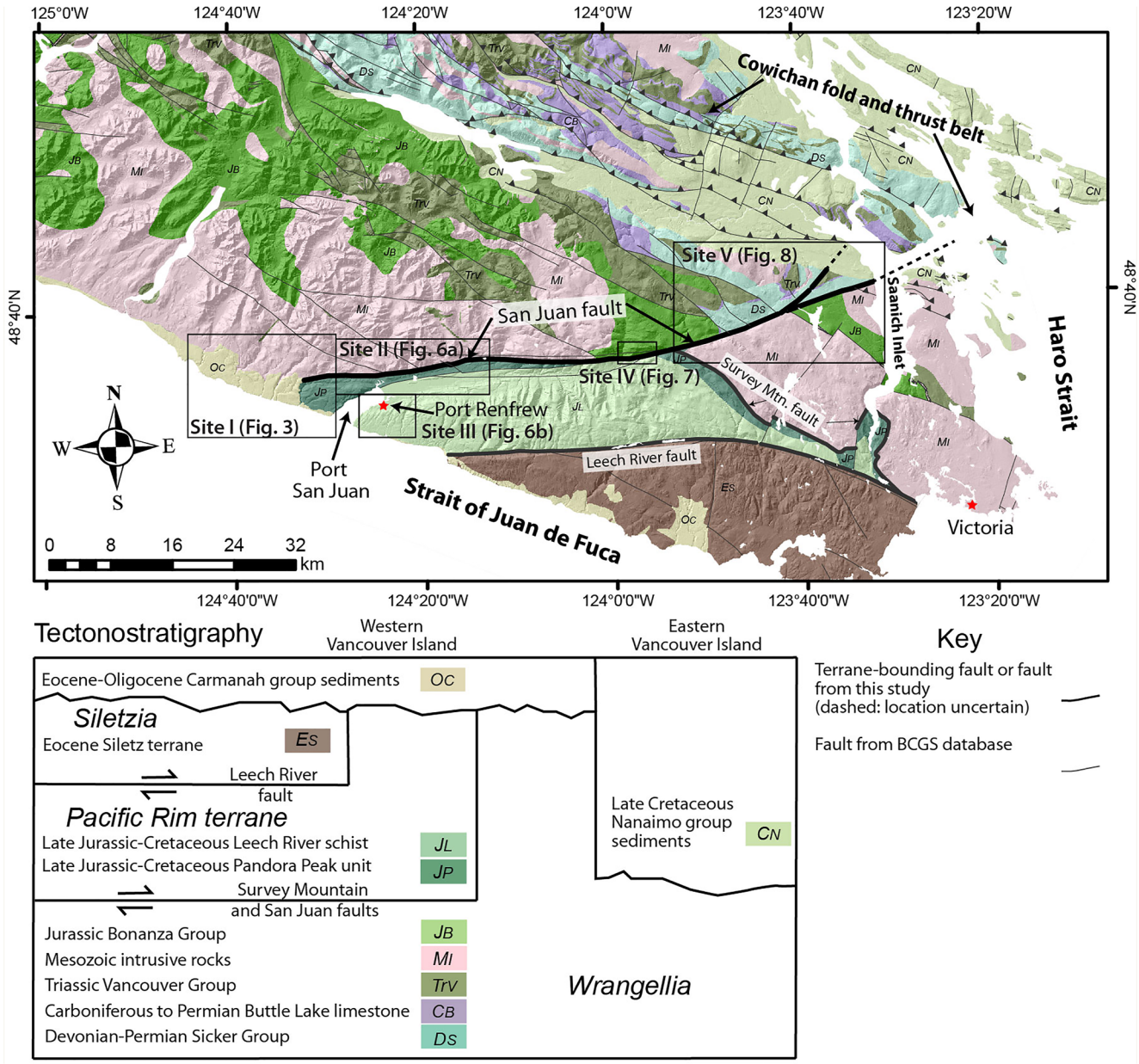

Figure 2. Bedrock geology of southern Vancouver Island and Site I–V locations. Thrust faults are shown in the Cowichan fold and thrust belt (England & Calon, 1991). Legend shows tectono-stratigraphic relationships of geologic units and terranes. Bedrock faults and geology are adapted from the British Columbia Geological Survey (BCGS) map compilation by Cui et al. (2017).

Chuckanut Formation, as well as the basement rocks of Wrangellia and the Pacific Rim terrane (Figures 1 and 2; Eddy et al., 2017; England & Calon, 1991; Johnson et al., 1996; Johnston & Acton, 2003; Massey, 1986; McCrory & Wilson, 2013; Wells et al., 2014). To the south of the Cowichan fold and thrust belt, accretion of Siletzia is thought to have resulted in folding of sediments in the Swauk basin and their underlying basement terranes, and right-lateral offset and the formation of sedimentary basins on the north-south striking Fraser–Straight Creek fault (Figure 1; Donaghy et al., 2021; Eddy et al., 2016; Miller et al., 2016).

Deposition of the late Eocene–Oligocene Carmanah Group strata, now exposed along the west coast of Vancouver Island (Figure 2), began after the Siletzia accretion (e.g., Garver & Brandon, 1994; Johns et al., 2012; Tiffin et al., 1972; Yorath, 1980). These marine clastic sediments unconformably overlie both Wrangellia and Pacific Rim terrane basement, and are exposed up to ~6 km inland from the west coast near the western extent of the

SJF (Clapp & Cooke, 1917). They constitute the basal stratigraphy of a >3,000 m-thick forearc basin sequence (Hyndman et al., 1990; Yorath, 1980) of fossiliferous interbedded sandstones, siltstones and minor conglomerates (Cameron, 1980; Clapp & Cooke, 1917; Jeletzky, 1954; Narayan et al., 2005). The Carmanah Group has been divided into three separate units, from oldest to youngest: the Escalante, Hesquiat, and Sooke Formations (Cameron, 1980; Clapp & Cooke, 1917; Jeletzky, 1954; Johns et al., 2012; Muller et al., 1981; Narayan et al., 2005). This sedimentary sequence is interpreted as being deposited in an upper bathyal-lower neritic (Hesquiat and Escalante) to inner neritic-littoral environment (Sooke), with an overall regression in relative sea level (Cameron, 1980; Jeletzky, 1954; Narayan et al., 2005; Prothero et al., 2008; Tiffin et al., 1972). Biostratigraphy (Cameron, 1980; Johns et al., 2012; Narayan et al., 2005; Tiffin et al., 1972), Sr isotope stratigraphy (Johns et al., 2012), and paleomagnetism (Prothero et al., 2008) place the Carmanah Group as late Eocene–early Oligocene in age, with the Eocene-Oligocene boundary occurring in the Hesquiat Formation.

3. The SJF

The present surface trace of the SJF is west-to southwest-striking, and transects southern Vancouver Island for ~80 km (Figure 2). The western portion of the SJF juxtaposes metasedimentary rocks of the Pacific Rim terrane with Paleozoic and Mesozoic island arc-associated rocks of Wrangellia (Rusmore & Cowan, 1985). East of the Survey Mountain fault, which splays off the SJF to the southeast, the SJF offsets different units of the Wrangellia terrane. Carmanah Group sedimentary strata are suggested to non-conformably overlie the fault at the far western extent of the SJF (Fairchild & Cowan, 1982; Rusmore & Cowan, 1985). However, before this study, detailed mapping has yet to precisely determine the cross-cutting relations between the SJF and the Carmanah Group. At its far eastern extent, the SJF intersects Cretaceous marine sediment of the Nanaimo Group; however, its stratigraphic relation with these sediments is obscured by Quaternary sedimentary cover (Figure 2; England & Calon, 1991).

Only a few details on the orientation, timing, and kinematics of the SJF are presented in previous literature. Rusmore and Cowan (1985) describe the fault as a steeply dipping ~75 m-wide zone of cataclasite, and seismic reflection data also show the SJF as a steeply dipping crustal structure (Clowes et al., 1987). Although no direct observations of the fault's kinematics have been reported several hypotheses regarding its kinematics have been proposed. High-P, low-T metamorphism of the Pandora Peak unit in the Late Cretaceous between 99 and 83 Ma, has been used as evidence that the SJF accommodated underplating along a subduction thrust (Brandon, 1989b; MacLeod et al., 1977; Muller, 1977). However, different metamorphic assemblages of the Pandora Peak unit and Wrangellia across the SJF led (Rusmore & Cowan, 1985) to conclude that juxtaposition of the Pandora Peak unit and Wrangellia occurred along a high-angle reverse or left-lateral fault after subduction-related metamorphism. Abrupt facies changes and the petrography of sediments formed marginal to the SJF have been used to imply right-lateral motion along the SJF during juxtaposition of Wrangellia and the Pacific Rim terrane (Johnson, 1984a). Finally, the SJF has also been hypothesized to be optimally oriented as a left-lateral fault during Eocene accretion of the Siletzia oceanic plateau (Figure 1, England & Calon, 1991; Fairchild & Cowan, 1982).

Northeast-southwest shortening in the Leech River Complex and the Cowichan fold and thrust belt during Eocene accretion of Siletzia has been used to speculate that the SJF may have accommodated left-lateral slip during the Eocene (Fairchild & Cowan, 1982), which may have taken the form of a tear fault or oblique ramp that soles into the Cowichan fold and thrust belt (England & Calon, 1991). The left-lateral hypotheses are consistent with bedrock geologic maps that portray ~60 km of apparent left-lateral offset of Wrangellia rocks (Figure 2, DeBari et al., 1999; Muller, 1977). However, no direct correlation of structures within Wrangellia has been documented across the SJF.

Post-Eocene slip of the SJF has previously been ruled out due to a lack of evidence for strike-slip faulting in the overlying Carmanah Group sediments (e.g., Fairchild & Cowan, 1982; Rusmore & Cowan, 1985). However, Holocene-active oblique right-lateral slip on the Leech River fault, only 10–25 km south of the SJF, has been recently documented (Harrichhausen et al., 2021; Morell et al., 2018, 2017). Therefore, detailed stratigraphic and structural analyses of the Carmanah Group sediments that directly overlie the SJF are needed to determine if the SJF has been reactivated since the Eocene.

4. Methods

4.1. Fault Geometry and Kinematics

To constrain fault geometry and kinematics, we conducted detailed geologic and structural mapping at 5 sites (Sites I–V) along the SJF and related structures (Figure 2). Dense vegetation limits outcrops to road cuts, quarries, creeks, and exposed beach platforms. We measured fault plane orientations and associated slickenlines from these outcrops, along with the orientations of bedding and foliation planes. Stereonet projections of these orientations were plotted and analyzed using the Stereonet 10.1.6 software (Allmendinger et al., 2011; Cardozo & Allmendinger, 2013). Tabulated structural data are provided in a data repository (Harrichhausen et al., 2022).

Slickenlines were used to determine brittle fault kinematics (e.g., Marrett & Allmendinger, 1991; Riller et al., 2017). Fault slip inversions from measurements within a fault zone relate to local strain, and can be used to infer the kinematics of a nearby master fault (Riller et al., 2017). We used criteria such as slickenfibers (e.g., Fagereng et al., 2011), and concentric markers, fractures, steps, and trailed material, described in Doblas (1998), where offset markers were not visible. We measured 836 fault planes and ~60%, or 494 of those planes had kinematic indicators where both a rake and slip sense could be determined. The most common criteria for evaluating slip sense were slickenfibers, offset of bedding planes, steps, and riedel shears. Fault planes with slickenlines were mapped and measured at outcrop scale, and were grouped into populations based on variables such as outcrop location, fault plane strike, and lithology. Further site specific explanations for grouping of faults are reported in the results section. The principal kinematic axes (incremental strain axes) and *P*- and *T*-dihedra for each fault plane were calculated using FaultKin 8.1.2 software (Allmendinger et al., 2011; Marrett & Allmendinger, 1990). We then used FaultKin to determine the principal kinematic axes for each population of faults and associated fault plane solutions using a linked Bingham analysis of the *P*- and *T*-axes (Betka et al., 2016; Marrett & Allmendinger, 1991). For each data set, we used the *Max Compatible Faults* algorithm to remove faults with *P*-dihedra that did not encompass the bulk shortening axis of the sample set (e.g., Allmendinger et al., 1989). We interpret these remaining data, which constitute ~22% of the total data set, to represent faults that may have formed during a different deformation event, or were measured from fault slickenlines with ambiguous kinematic indicators (e.g., Doblas, 1998) that could result in misinterpretation of slip sense. For example, certain steps and concentric markers can potentially indicate two opposite slip senses (Doblas, 1998). Because of these possibilities, we consider these measurements as outliers or scatter in our data, and they are excluded from our kinematic inversions. Tabulated fault plane and slickenline data used for kinematic inversions are provided in a data repository (Harrichhausen et al., 2022).

4.2. Timing of Fault Slip

To constrain the minimum age of fault slip on the SJF, we mapped and dated the Carmanah Group marine sediments to test if these sediments were deposited after slip on the SJF. We examined sedimentary strata on exposed platforms and beach cliffs along the southwest coast of Vancouver Island to determine sediment lithology, structures, and depositional environments. We used structural contour mapping (e.g., Groshong, 2006) of the basal contact of the sediments, identified at seven outcrops, to estimate the extent of the sediments in areas with little exposure. We also used this method to interpolate the maximum elevation of this unit where no outcrop could be accessed, and the maximum thickness of the unit at the coast in the map area.

We used Sr isotope stratigraphy ages of an abundant foraminifer species from samples collected from the Carmanah Group stratigraphy to determine the depositional age of the sediments. In preparation for Sr isotope analyses, the same species of foraminifers were hand-picked from a specific sample residue by selecting the most abundant and diagnostic species with the least diagenetic and thermal alteration of specimens. Selected specimens from the study area had some diagenetic alteration of the external foraminifer shell material where they showed chalky white outer shell material. Some specimens were selected that had more interior depth with much less diagenetic alteration. This was done in order to achieve results that reflected unaltered material, instead of a mixture of interior and exterior shell material. Ten to seventy foraminifers were selected from each sample, depending on the size and number of specimens available. Although we collected 49 samples, only two samples had sufficient specimens to provide internally consistent Sr isotope ages.

$^{87/86}$Sr isotope analyses were completed at the University of Waterloo by the Thermal Ionization Mass Spectrometry Facility, using a Thermo Finnigan Triton instrument. A reported result for $^{87/86}$Sr was obtained using 120

measurements, with raw data normalized using $^{88/86}Sr = 8.375209$ and corrected against the NIST987 standard reference material where $^{87/86}Sr = 0.710248$ (McArthur et al., 2020). $^{87/86}Sr$ results are presented to six decimal points as raw normalized to NIST-SRM-987 and USGS EN-1 standards. Sr isotope age is determined using a McArthur LOWESS 5 Best Fit 26 03 13 look-up table (McArthur et al., 2020) that includes minimum, mean, and maximum values and gives Series/Epoch and a geologic age. The error for the Sr isotope age is calculated by subtracting or adding each maximum or minimum look-up age table result from the mean. We report the age for our sample as the range between the minimum and maximum ages calculated using both standards. Detailed Sr isotope data are provided in a data repository (Harrichhausen et al., 2022).

5. Results

We first describe the stratigraphy and age constraints of the Carmanah Group sediments that have been suggested to overlie the westernmost ~4 km of the SJF's surface trace at Site I (Figure 2). We then describe deformation observed along the SJF and related structures from west to east at Sites I–V.

5.1. Site I Stratigraphy

The Carmanah Group at Site I is a greater than 300 m-thick, fining-upwards sequence of clastic marine sediments that non-conformably overlies the basement Mesozoic intrusive rocks and the Pandora Peak unit, as well as the SJF (Figure 3). These sediments outcrop at sea level along a ~50–100 m-wide wave-cut platform with a <40 m high sea cliff, up to an elevation of ~400 m inland. Strata in this unit dip uniformly 3°–20° toward the southwest (Figure 3), except for locally steep cross-stratification and bedding planes near the basal contact or steep normal faults. From southeast to northwest along the coastline, rocks successively higher in the stratigraphy and a thicker stratigraphic section are exposed. Five stratigraphic sections (Figures S1–S5 in Supporting Information S1), at locations V through Z on Figure 3, were used to construct a generalized stratigraphic sequence of the Carmanah Group sediments in the study area (Figure 4).

The basal contact between the basement terranes and the Carmanah Group sediments is erosional, and overlain by boulder-cobble conglomerate with a coarse sand to granule matrix containing abundant shell fragments (Figure 5a). We identified the basal contact of the Carmanah Group at seven locations, and contour mapping suggests that the attitude of the basal contact dips gently southwest (~8°) with similar dip to overlying strata (e.g., Figure 5a). The basal conglomerate ranges from ~0.5–1 m thick at Owen Point (V, Figure 3), to >10 m thick along upper Walbran Creek and where it is exposed at higher elevations (~400 m) north of the modern coastline (Figure 3).

A fining-upwards package of predominantly medium and fine-grained sandstone conformably overlies the basal conglomerate (Figure 4). Immediately above the conglomerate are ~10–25 m of 1–2 m-thick fining-upward sequences containing medium-to coarse-grained calcite-cemented sandstone with hummocky and uni-directional cross-stratification (Figure 5b), abundant shell fragments, and decimeter-scale burrows (Figure 5c). These fining-upwards sequences are conformably overlain by ~10 m of massive to faintly bedded, fine-to medium-grained sandstone containing abundant 0.1–0.5 m-thick oblate concretions encasing gastropod, bivalve, scaphopod, and plant fossils (Figures 5d and 5e). Above the concretion-bearing sandstone beds are 1–3 cm-thick beds of fine-to medium-grained sandstone with discontinuous cm-thick organic-rich seams (Figure 5f). Hummocky cross-stratification and abundant broken shells indicate that the sediments nearer to the base of the sequence were likely deposited in a high-energy environment above wave base, while the organic-rich seams higher in the stratigraphy may indicate deposition in deeper water, such as a coastal lagoon environment.

Greater than 100 m above the basal contact (Figure 4), the stratigraphy is composed of well-bedded fine-to medium-grained lithic sandstone containing abundant fragments of bivalve, scaphopod, and gastropod shells. The fine-to medium-grained sandstone is cut by >2 m-thick channel deposits of medium to coarse sand that strike 190°–220° (Figure 5g), which is perpendicular to the modern coast line.

Sr isotope age results, although limited, are consistent with a late Eocene–early Oligocene depositional age for the lower 60 m of the Carmanah Group at Site I. *Cibicides* sp. 1 foraminifers from sample Q2-15 collected in Quarry 2 (Location Q2, Figure 3), suggest a mean age of 33.75 ± 0.52 Ma when using the USGS EN-1 standard and 33.96 ± 0.51 Ma when using the NIST-987 standard (Table 1). Using the entire range of ages from

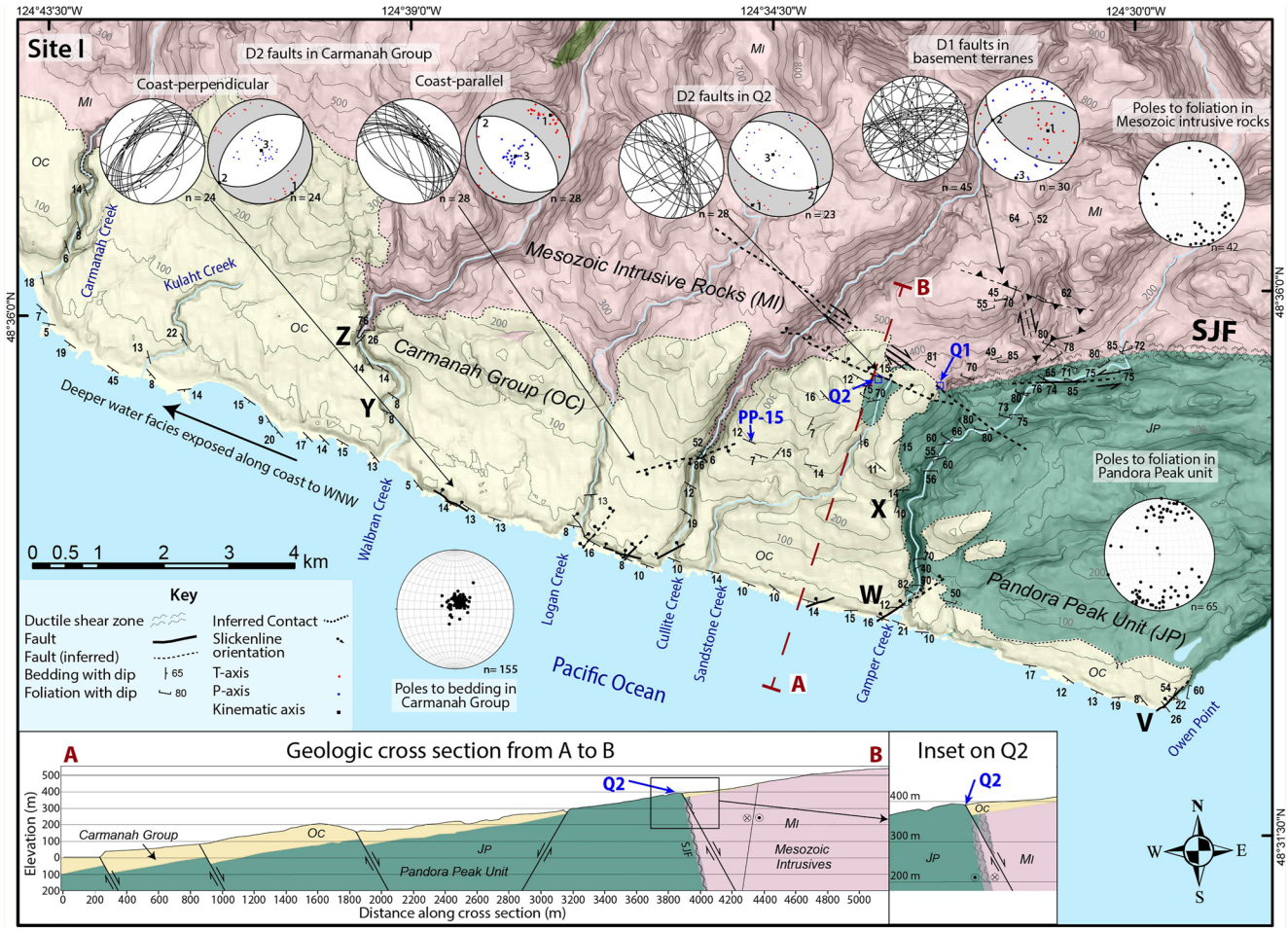

Figure 3. Bedrock geology overlain on slope map of Site I (location shown in Figure 2). Geologic cross-section (a–b) shown at bottom left. Q2 and *V*–*Z* denote locations of stratigraphic columns (Figure 4). Inset maps of Quarry 1 (Q1) and Quarry 2 (Q2) are shown in (Figure S7 in Supporting Information S1). Lower hemisphere equal area stereonet projections at top of map show fault planes, slickenlines, *P*- and *T*-axes, linked Bingham fault plane solutions, and principal strain axes (1: maximum, 2: intermediate, 3: minimum) of brittle deformation events 1 (D1) and 2 (D2) from specified locations. *n* = number of compatible slickenline orientations used in kinematic inversion. Tabulated kinematic axes are shown in Table 2. Stereonet projections of poles to bedding in the Carmanah Group marine sediments and poles to foliation in the Mesozoic intrusive rocks and the Pandora Peak unit are also shown. Geology legend from Figure 2.

our measurements, we determine that the foraminifers in this sample were deposited between 34.45 Ma and 33.25 Ma. Sr ages obtained from the bivalve fragments and *Quinqueloculina* sp. 1 foraminifers (Table 1) at Q2 and W yielded ages that differ significantly from previous Eocene-Oligocene age estimates of the Carmanah group (Cameron, 1980; Johns et al., 2012; Narayan et al., 2005; Prothero et al., 2008; Tiffin et al., 1972), suggesting either significant diagenetic alteration of these fossils, a terrestrial or other source of Sr, and/or reworking of older fossils in the sediments of the Carmanah Group preventing accurate Sr isotope dating (e.g., Mesozoic ages in Table 1). Our structural contour mapping places the Q2 sample between ~10 and ~40 m above the basal contact of the Carmanah Group. Given the similar lithologies suggesting a continental shelf depositional environment we document at several locations near the base of the Carmanah Group at Site I (Figures S1–S5 in Supporting Information S1), we interpret this age to provide a generalized constraint on the depositional age that is consistent with published age estimates of the Hesquiat Formation (Cameron, 1980; Johns et al., 2012; Narayan et al., 2005; Prothero et al., 2008; Tiffin et al., 1972).

5.2. Deformation

The structure of the SJF varies from west to east along its surface trace. At its western extent at Sites I and II (Figure 2), a wide, 1 km-wide brittle fault zone overprints ductile deformation. Toward the east at Sites IV and

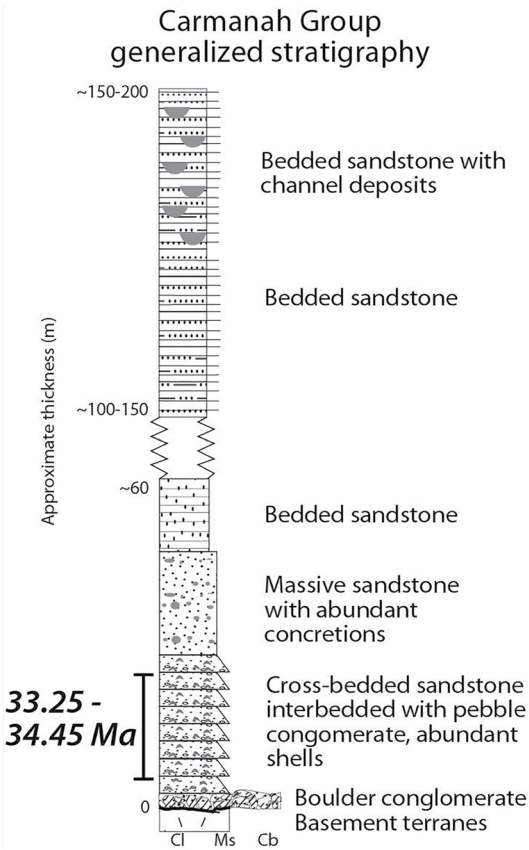

Figure 4. Generalized stratigraphic section showing clastic sedimentary sequence of the Carmanah Group at Site I. Basal portion section is based on sedimentary stratigraphy at Owen Point. Conglomerates near the basal contact are thicker at higher elevations (e.g., upper Walbran Creek). The interpreted approximate stratigraphic range of Sample Q2-15, with its associated Sr isotope age is shown. The missing section is a result of a lack of outcrop between upper and lower Walbran Creek. We estimate the thickness of the missing section using contour mapping to be ~40–90 m thick. The generalized section is based on detailed stratigraphic columns shown in Figures S1–S5 in Supporting Information S1. The locations of these detailed stratigraphic columns, Q2 and *V-Z*, are on Figure 3. Grain size abbreviations: Cl, clay; Ms, medium sand; Cb, cobble.

V, the brittle SJF is still observed, but there is no obvious ductile shear zone. We present the structural observations at each one of these sites, along with Site III, which lies south of the main SJF fault strand. Fault plane slickenline kinematic inversions of fault populations from each study site are shown in Table 2. The kinematic axes 1, 2, and, 3 in Table 2 are the maximum, intermediate, and minimum principal strain axes (with respect to extension of an ellipsoid), respectively, from each kinematic inversion.

5.2.1. Site I

5.2.1.1. Ductile Deformation at Site I

The SJF at Site I is a ~1 km-wide brittle-ductile shear zone that offsets Mesozoic intrusive rocks of Wrangellia to the north against meta-sediments and volcanics of the Pandora Peak unit in the Pacific Rim terrane to the south (Figure 3). Foliation associated with ductile deformation in the Mesozoic intrusive rocks is primarily steeply north-dipping, west-southwest-striking, and sub-parallel with the strike of the SJF at Site I (Figure 3). In the Pandora Peak unit, the foliation is steeply north-dipping and strikes east-west. It cross-cuts folded primary compositional layering or bedding that is predominantly steeply north-dipping and west- northwest-striking (Figure 3). Gently dipping surfaces exposing σ-clasts, asymmetric folds, and minor offsets of compositional layering and foliation indicate apparent left-lateral ductile shear sense in the Pandora Peak unit (Figure S6 in Supporting Information S1); however, a sense of slip was not apparent in the shear fabric of the Mesozoic intrusive rocks. Quartz-calcite cemented fault zones with a fine-grained scaly fabric, defined as a macroscopic fabric formed by pervasive anastomosing surfaces cross-cutting argillaceous or clay-rich material (e.g., Bradbury et al., 2011; Cowan, 1985; Kirkpatrick et al., 2015; J. C. Moore et al., 1986; Vannucchi, Maltman, et al., 2003), cross-cut the ductile shear zone between these units. The largest m-scale cemented fault zones are subvertical and west- northwest-striking.

5.2.1.2. Brittle Deformation at Site I

Evidence for two distinct brittle deformation events was observed at Site I, an older event that only deforms the basement rocks, and a younger event that deforms all strata including the overlying Carmanah Group. Faulting associated with the first, older event cross-cuts the ductile SJF, the Mesozoic intrusive rocks, and the Pandora Peak unit (Figure 3). The faults consist of cataclasite-rich m-wide reverse faults and narrow (cm-scale) planar strike-slip faults. The reverse faults are typically moderately to steeply north-dipping, and have 0.1–2 m-thick fault cores consisting of fault gouge. These fault cores are surrounded by >2 m-thick damage zones with quartz, calcite, epidote, and chlorite slickenfiber growth on fault planes (e.g., Figure 5h). The thinner planar faults typically are subvertical west-striking left-lateral faults, and northwest-to north-striking right-lateral faults. However, we observed one wider (~2 m-wide) northwest-striking right-lateral fault that offsets the SJF by <1 km (exposed at Q1, Figure 3; Figure S7 in Supporting Information S1). This fault is oriented approximately 45° to the main strand of the SJF.

Kinematic inversion of the faults representing this older deformation event affecting the basement terranes indicates predominantly reverse slip with a lesser left-lateral strike-slip component. This inversion implies a north-northeast-south-southwest maximum shortening direction (Table 2; D1 stereonets, Figure 3). Right-lateral slip on west- northwest-striking subvertical faults, including the 2 m-wide right-lateral fault that offsets the ductile SJF at Q1, is kinematically consistent with this inversion.

The second deformation event, deforming both the basement terranes and the overlying Carmanah Group sediments, consists of two populations of normal faults with minor offsets. The first population is a set of coast-parallel (east-southeast to west-northwest) faults that predominantly dip ~60° to the northeast. The second is a set of

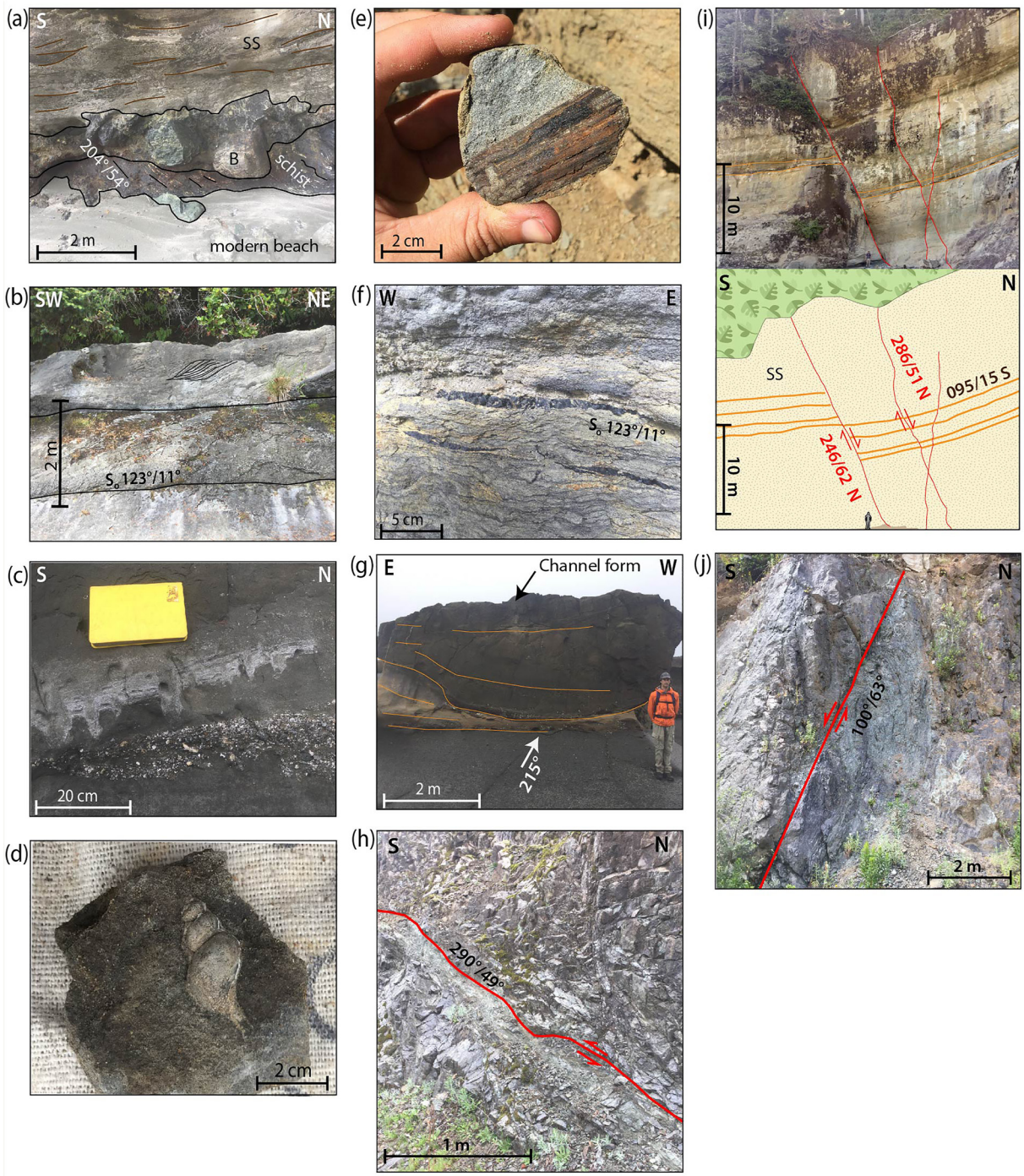

Figure 5. Photos of sedimentary structures, fossils, and faults at Site I (Figure 3). (a) Boulder conglomerate (b) and gently dipping sandstone (SS) overlying schist of the Pandora Peak unit at basal contact of the Carmanah Group (V, Figure 3). (b) Meter-scale planar beds of medium-grained lithic sandstone with internal cross-stratification indicating a current flow from northeast (right) to southwest (left) (V, Figure 3). (c) Interbedded medium and coarse sandstone with hummocky cross-stratification, abundant broken shells and burrows. Photo taken at 22 m in Camper Creek column (W, Figure 3, Figure S3 in Supporting Information S1). (d) Two centimeters-wide gastropod collected from concretion-bearing massive sandstone at elevation of 250 m between Cullite and Sandstone Creeks. (e) Fibrous plant material found at same location as (d). (f) cm-scale carbon-rich layers interbedded with fine-medium sandstone. Located on coastline between Location W and Location V. (g) Four meters-wide medium-grained sandstone channel form deposited in fine-to medium-grained sandstone striking toward 215°. Photo taken on coast between Kulaht and Walbran Creeks. (h) Twenty to fifty centimeters-thick reverse fault cross-cutting intensely sheared Mesozoic intrusive rock. Photo taken at northwest-striking reverse fault ~1 km north of the SJF (Figure 3). (i) Photograph (top) and interpretation (bottom) of normal faults cross-cutting shallowly south to southwest-dipping medium-grained m-scale beds of marine sandstone at the mouth of Cullite Creek. (j) Planar normal fault in Quarry 2 (Q2) cross-cutting mylonite and chert of the Pandora Peak unit.

Table 1
Sr Age Results for Foraminiferal Species at Site I

Site	Sample	Species	n[a]	Run #	Standard	$^{86/87}$Sr	2σ	Age min (Ma)[b,c]	Age mean (Ma)[b,c]	Age max (Ma)[b,c]	Epoch
Q2	Q2-15	*Cibicides* sp. 1	120	434,155	USGS EN-1	0.707835	0.000018	**33.58**	**33.75**	**33.90**	Early Oligocene
Q2	Q2-15	*Cibicides* sp. 1	120	434,155	USGS EN-1	0.707853	0.000018	**33.25**	**33.39**	**33.54**	Early Oligocene
Q2	Q2-15	*Cibicides* sp. 1	120	434,155	USGS EN-1	0.707816	0.000018	**33.96**	**34.11**	**34.27**	Late Eocene
Q2	Q2-15	*Cibicides* sp. 1	120	434,155	NIST-987	0.707824	0.000017	**33.80**	**33.96**	**34.11**	Early Oligocene
Q2	Q2-15	*Cibicides* sp. 1	120	434,155	NIST-987	0.707841	0.000017	**33.45**	**33.61**	**33.79**	Early Oligocene
Q2	Q2-15	*Cibicides* sp. 1	120	434,155	NIST-987	0.707807	0.000017	**34.15**	**34.30**	**34.45**	Late Eocene
W	W-8	*Quinqueloculina* sp. 1	59	434,151	USGS EN-1	0.707343	0.000016	88.80	88.98	89.15	Late Cretaceous
W	W-8	*Quinqueloculina* sp. 1	59	434,151	NIST-987	0.707325	0.000015	89.38	89.53	89.65	Late Cretaceous
W	W-8	bivalve, shell fragments, tubes	23	434,152	USGS EN-1	0.707071	0.000016	150.50	150.65	150.75	Late Jurassic
W	W-8	bivalve, shell fragments, tubes	23	434,152	NIST-987	0.707052	0.000016	151.20	151.30	151.40	Late Jurassic
Q2	Q2-15	*Quinqueloculina* sp. 1	10	434,153	USGS EN-1	0.706892	0.000028	156.45	156.75	157.00	Late Jurassic
Q2	Q2-15	*Quinqueloculina* sp. 1	10	434,153	NIST-987	0.706892	0.000027	156.45	156.75	157.00	Late Jurassic
Q2	Q2-15	bivalve, shell fragments, tubes	15	434,154	USGS EN-1	0.706814	0.000015	N/A	N/A	N/A	N/A
Q2	Q2-15	bivalve, shell fragments, tubes	15	434,154	NIST-987	0.706796	0.000015	N/A	N/A	N/A	N/A

[a]n = number of specimens. [b]Ages derived from the McArthur Sr lookup table: LOWESS (26 March 2013) McArthur et al. (2020) best fit. [c]Bolded ages used in interpretation. The remaining ages represent over-printed signatures.

Table 2
Kinematic Axes Derived From Inversion of Fault Slickenline Measurements

Site	Domain	n_c[a]	n_i[b]	Kinematic axis 1[c]	Kinematic axis 2[c]	Kinematic axis 3[c]
I	D1 faults	30	15	57° → 095°	34° → 285°	04° → 192°
I	D2 faults, Q2	23	5	03° → 210°	19° → 119°	71° → 308°
I	Carmanah Group coast-perpendicular	24	0	00° → 143°	02° → 233°	88° → 048°
I	Carmanah Group coast-parallel	28	0	07° → 042°	03° → 312°	82° → 203°
II	Domain 1 stereonet A	28	4	32° → 103°	58° → 273°	04° → 010°
II	Domain 2 stereonet B	12	3	05° → 289°	58° → 026°	32° → 196°
II	Domain 2 stereonet C	31	8	03° → 101°	01° → 011°	87° → 262°
II	Domain 3 stereonet D	16	5	05° → 298°	78° → 052°	11° → 207°
II	Domain 3 stereonet E	12	2	23° → 099°	03° → 190°	67° → 287°
II	Domain 4 stereonet F	15	0	21° → 258°	64° → 118°	15° → 354°
II	Domain 4 stereonet G	3	0	67° → 191°	22° → 026°	06° → 294°
III	Northwest (top left) stereonet	3	0	11° → 310°	56° → 058°	31° → 213°
III	West (middle left) stereonet	4	0	08° → 262°	82° → 070°	02° → 172°
III	Northeast (top right) stereonet	5	0	00° → 337°	10° → 247°	80° → 068°
III	Southeast (bottom) stereonet	7	1	21° → 284°	61° → 059°	19° → 187°
IV	Not including northern thrust	51	20	09° → 121°	66° → 023°	22° → 027°
V	Main shear zone	21	0	71° → 233°	16° → 085°	11° → 356°
V	Outside of main shear zone	60	19	73° → 297°	17° → 105°	03° → 196°
V	West	11	2	47° → 105°	43° → 288°	02° → 197°

[a]n_c = number of compatible measurements. [b]n_i = number of excluded measurements. [c]Plunge → trend of axis.

approximately coast-perpendicular (southwest-northeast) faults that dip ~60° to the northwest and southeast. The coast-parallel faults cross-cut the coast-perpendicular faults at two locations; however, the cross-cutting relationship between these two populations is unclear at other locations.

A coast-parallel normal fault offsetting the overlying Carmanah Group against the Pandora Peak unit is exposed at Q2 (Figure 3; Figure S7 in Supporting Information S1). This fault is steeply northeast-dipping, northwest-striking, and has a fault core that is ~0.5 m wide and composed of calcite-cemented cataclasite and mylonite clasts. Planar, moderately to steeply dipping, northwest-striking normal faults make up the majority of the faults in the footwall (Pandora Peak unit). These faults are planar with narrow (<10 cm) fault cores containing calcite veins (e.g., Figure 5j).

Both populations of normal faults cross-cutting the Carmanah Group are commonly narrow (<10 cm) and planar, and also contain minor calcite veins (Figure 5i). They commonly form several m-spaced bookshelf sets and grabens. Apparent normal offset on most faults is minor (e.g., <10 m, Figure 5i); however, several faults have apparent offsets greater than the size of the outcrop (~20 m), including faults which also offset the basement terranes. Despite the lack of slip-constraint on some of these normal faults, we did not observe any significant offset of lithological units and contacts (Figure 3) that would suggest major displacements (e.g., >100 m).

Slickenline measurements on the fault planes from the second deformation event were also used for kinematic inversions (D2 stereonets, Figure 3; Table 2). Fault slickenline measurements indicate that both populations of faults observed in the Carmanah Group record normal dip-slip fault motion with rakes of 60°–90°. The coast-parallel population accommodated southwest-northeast extension and the coast-perpendicular set accommodated northwest-southeast extension. In addition, kinematic inversion of 23 predominantly northwest-striking normal faults cross-cutting the Pandora Peak unit in Quarry 2 indicates normal faulting with approximately the same kinematics as the coast-parallel normal faults in the Carmanah Group (D2 stereonets, Figure 3; Table 2).

5.2.2. Site II

Site II is immediately east of Site I and north of the town of Port Renfrew (Figure 2). Here, the SJF is a <1 km-wide zone of distributed brittle and ductile deformation that juxtaposes fine- to coarse-grained gabbro, diorite, and marble of Wrangellia to the north with interbedded metavolcanics, schist, chert and minor limestone of the Pandora Peak unit in the Pacific Rim terrane to the south. The Pandora Peak unit, which is a ~2 km-wide west-trending swath in map view, is in turn in contact with schist of the Leech River Complex, also within the Pacific Rim terrane (Figure 2). Similar to Site I, there are multiple generations of deformation recorded at Site II. Brittle-ductile deformation and oblique left-lateral faulting with a reverse component characterizes deformation recorded in the entire map area. A generation of normal faults in the Pandora Peak unit (Pacific Rim terrane) is observed at two locations. Finally, reverse faults with a northwest-southeast maximum shortening direction are also observed at one location in Wrangellian intrusives.

5.2.2.1. Ductile Deformation at Site II

We recorded east- and west-striking foliation within all geologic units and steeply plunging folds in the Pandora Peak unit (Figure 6a). Foliation planes in all three units predominantly dip steeply north, consistent with a north-northeast-south-southwest shortening direction. Foliation attitudes measured in the Mesozoic intrusive rocks are variable and locally are aligned with local fault zones; however, plots of all poles to the foliation attitudes from this unit indicate foliation as moderate to steeply dipping and east-west striking (Figure 6a). Within the Pandora Peak unit, foliation planes consistently strike west and dip steeply to the north (Figure 6a). In the Leech River Complex, schist foliation trends west-northwest and dips moderately to steeply north, despite broadly folded foliation observed at some locations (Figure 6a). Chert bedding attitudes in the Pandora Peak unit are also predominantly steeply north-dipping and west-striking (Figure 6a); however, bedding also forms steeply plunging chevron folds with an interlimb angle of ~40°–90° (Figure S8 in Supporting Information S1).

5.2.2.2. Brittle Deformation at Site II

Brittle faulting along the SJF at Site II consists of a 30–50 m-wide main fault zone forming the contact between the Pandora Peak unit and the Mesozoic intrusive rocks (Figure 6a), and surrounding subsidiary faults. A dense brittle fault network deforms the entire ~2 km width of the Pandora Peak unit and cross-cuts rocks of the Leech River Complex and Wrangellia. The primary fault zone does not extend more than 500 m north of the Pandora Peak Unit—Wrangellia contact and its width within the Leech River Complex is unclear due to lack of exposure.

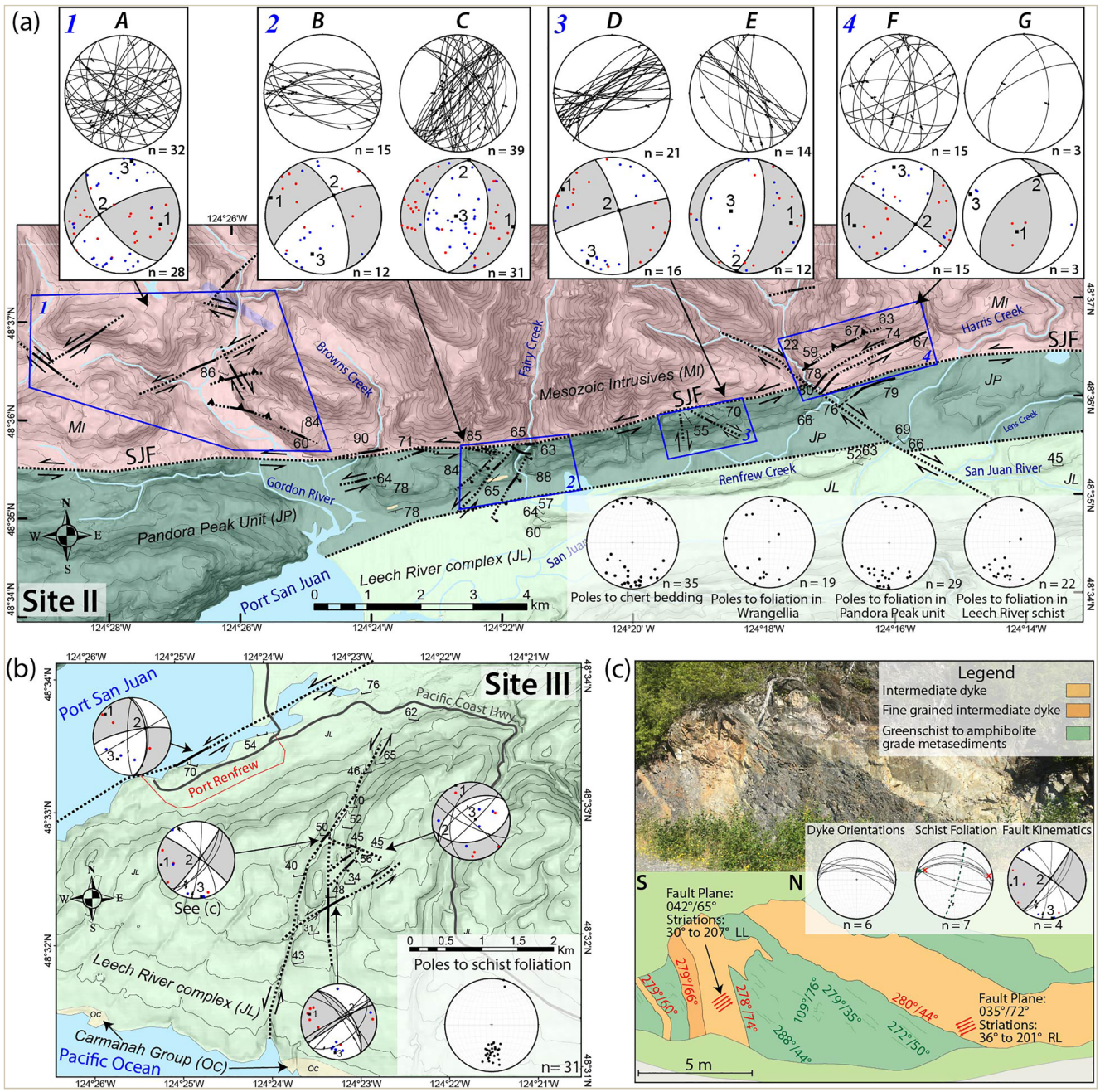

Figure 6. (a) Bedrock geology map of Site II. Fault domains 1–4 are shown in blue. Fault planes and slickenlines, and kinematic inversion models (using *n* compatible measurements) from each fault domain are shown in stereonet projections on map. Stereonet projections at bottom (from left to right) show poles to chert bedding and foliation in the three lithological units. (b) Bedrock geology overlain on slope map of Site III. Small stereonet projections show kinematic inversions for fault slickenline measurements from outcrops indicated by arrows. Poles of east- and west-striking, moderately north-dipping foliation planes measured in the map area are shown in the stereonet projection at bottom right. (c) Photograph (above) and interpretation (below) of dykes intruding Leech River Complex schist. Dyke orientations, schist foliation orientations, poles, and measured fold hinges, and fault plane and slickenline orientations with kinematic inversion are shown from left to right in the stereonet projections. Best-fit great circle (dashed green great circle) and β-axis (large green dot) approximate the fold hinge, which is sub-parallel with the measured fold hinges (large red Xs). Tabulated kinematic axes for (a and b) are shown in Table 2. Geologic legend for (a and b) is from Figure 2 and key for (a and b) is from Figure 3. Geologic contacts for (a and b) adapted from BCGS map compilation by Cui et al. (2017). Fifty-meter elevation contour spacing for (a and b).

The fault is exposed at three locations and is a steeply dipping ~30–50 m-wide zone of intensely sheared, dark, fine-grained cataclasite. It exhibits anastomosing shear surfaces coated with graphite, calcite, epidote, and chlorite. As the rock texture is obliterated within the fault zone, we cannot confirm if this fault is developed predominantly within the Mesozoic intrusive rocks or the Pandora Peak unit.

Faults located in the Mesozoic intrusive rocks and Pandora Peak unit, away from the lithologic contact between the Pandora Peak unit and Wrangellia rocks, consist of brecciated wallrock, chlorite, and anastomosing shear surfaces that occasionally form a scaly fabric, and contain silty gouge cemented with calcite. Some fault damage zones also exhibit intense alteration to light gray clay and hematite. In some areas, faulted chert and siliceous sediments are overprinted by dense networks of quartz-calcite veins and exhibit evidence for silica flooding of the wallrock.

We extrapolated (along strike) the mapped major fault zones at Site II across areas with no exposure and found they form fault networks that could be separated into four separate fault domains, based on location, lithology, and predominant fault kinematics (Table 2; Figure 6a). In each domain, we observe left-lateral and oblique left-lateral strike-slip faults with northeast-southwest to north-south maximum horizontal shortening axes. In fault domain 1, variably striking oblique left-lateral and right-lateral faults, consistent with these shortening axes, cross-cut the Mesozoic intrusive rocks and marble observed north of the SJF (Stereonet A). In fault domains 2 and 3, moderately- to steeply dipping ~east-northeast and west-striking faults that cross-cut the Pandora Peak unit south of the SJF accommodate left-lateral oblique slip (Stereonets B and D). Finally, in fault domain 4, we observed <500 m of right-lateral offset of the SJF (Stereonet F) along a northwest-striking subvertical fault oriented approximately 40° to the main strand of the SJF. Despite the right-lateral slip sense, this fault is also consistent with the approximate north-south horizontal shortening axes observed in the other fault domains.

In addition, three of the fault domains have a population of oblique normal (domains 2 and 3) or thrust (domain 4) faults (Table 2; Figure 6a). In fault domain 2, a set of mostly north- northeast-striking oblique normal faults (Stereonet C), and in domain 3 north- northwest-striking oblique normal faults (Stereonet E), are indicative of east-northeast to west-northwest extension. Conversely in fault domain 4, we observe moderately dipping southwest-striking reverse faults cross-cutting the Mesozoic intrusive rocks (Stereonet G).

5.2.3. Site III

Site III lies within the Pacific Rim terrane, adjacent to and south of Site II. Here, steeply dipping northeast-striking brittle faults that branch southwards from the SJF cross-cut schistose foliation and intrusions in the Leech River Complex (Figure 6b). The intrusions are intermediate to felsic, ~1–15 m-wide, tabular bodies consisting of >80% light-colored aphanitic ground mass with mm-sized foliated biotite crystals (Figure 6c). These observations suggest that the intrusions are part of the ~51 Ma tonalite-trondhjemite-granodiorite of the Walker Creek unit (Groome et al., 2003). Moderately north-dipping west-striking foliation in the schist (Figure 6b) and cm-wide quartz-calcite veins are deformed by minor (~1 m wavelength) close folds that have west- northwest-trending subhorizontal fold axes (both measured hinges and calculated fold axes using a β point: Figure 6c). Aside from these folds we did not observe evidence for significant ductile deformation at Site III.

5.2.3.1. Brittle Deformation

We observe two populations of brittle faults at Site III, left-lateral strike-slip faults and normal faults. Steep northeast-striking strike-slip faults that cross-cut both the schist foliation and the dykes are up to 1 m in width, with calcite-cemented cataclasite-filled fault cores. Kinematic analyses of slickenfibers in the damage zones of these faults are consistent with left-lateral slip with north-south to northeast-southwest horizontal shortening axes (Figures 6b and 6c). The normal faults we observed are moderately dipping, northeast- and southwest-striking and accommodate northwest-southeast extension (Figure 6b). We did not observe cross-cutting relationships between the fault generations at this site, and therefore cannot determine the relative timing of each deformation event.

Relatively undeformed marine sandstone and conglomerate of the Carmanah Group non-conformably overlie the schist and intrusions along the southwest coast in the map area; however, its outcrop is limited to within ~500 m of the modern beach (Figure 6b). The small outcrop at this location limited observations of deformation recorded in the Carmanah Group at this site.

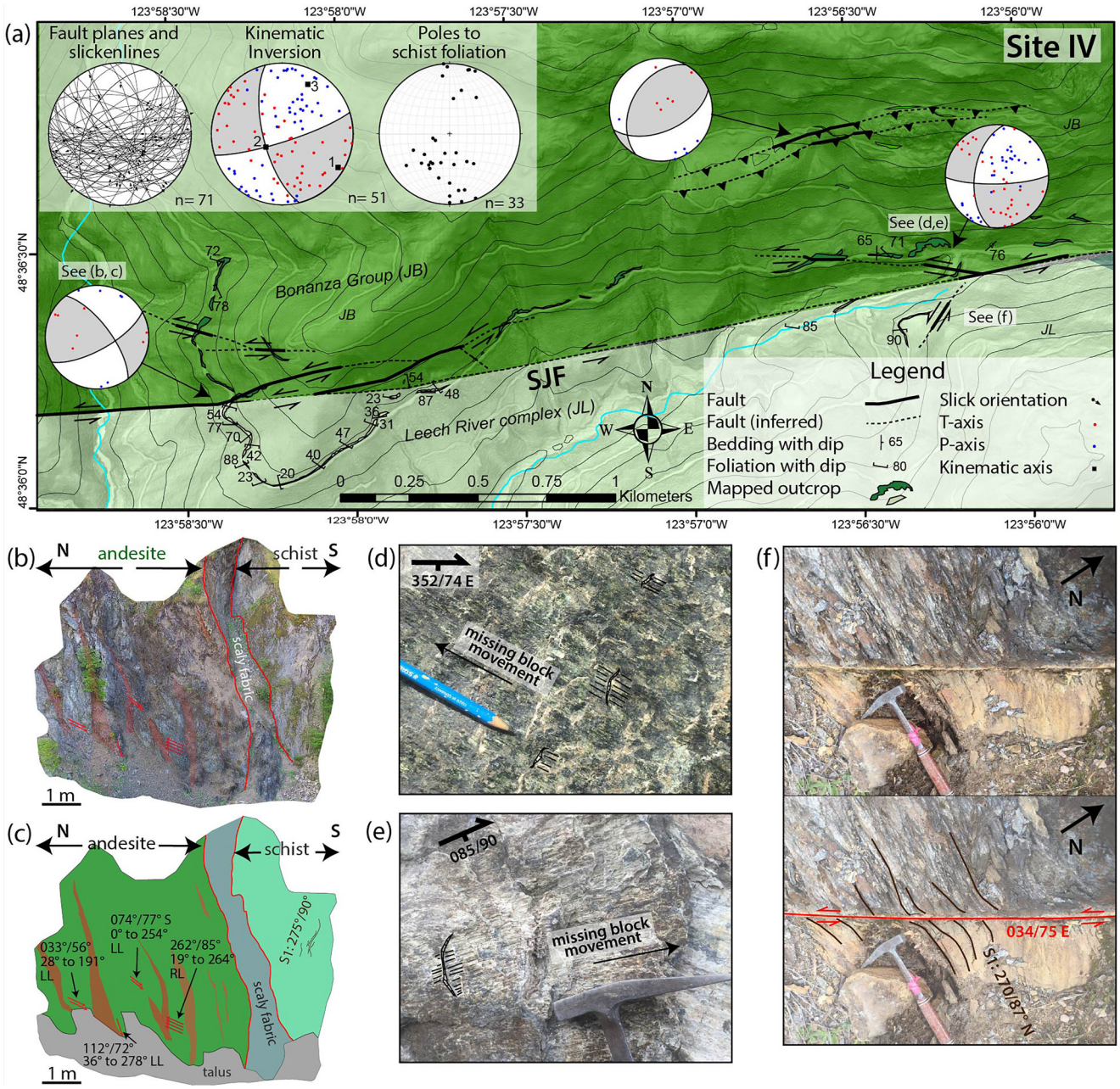

Figure 7. (a) Geology overlain on slope map of Site IV. Stereonet projections on the map show *T*- and *P*-axes and fault plane solutions for denoted locations. Stereonet projections at top left from left to right: fault planes and slickenlines within 500 m of the main strand of the SJF; *T*- and *P*-axes, kinematic axes, and linked Bingham fault plane solutions of 51 compatible faults; poles to schist foliation. Tabulated kinematic axes are shown in Table 2. Geologic legend is the same as Figure 2. Fifty meters-contour spacing. (b) Photomosaic showing the main terrane-juxtaposing fault at Site IV. (c) Interpretation of (b) with fault plane and slickenline orientations. LL, left-lateral slip sense, RL, right-lateral slip sense. (d–f) Congruous steps and slickenfibers formed on quartz, chlorite, epidote, and calcite coated slickenside surfaces indicating right-lateral slip in (d) and left-lateral slip in (e). (f) Uninterpreted photo (top) and interpreted photo (bottom) of drag folds formed in schist foliation indicating left-lateral slip.

5.2.4. Site IV

Site IV is located on the SJF ~16 km east of Site II and ~2 km west of the south-branching Survey Mountain fault (Figure 2). At Site IV, the SJF is a ~1 km-wide fault zone containing several 1–10 m-wide subvertical faults. The fault zone includes a main terrane-juxtaposing, brittle strand of the SJF, and several other major faults that obliquely branch off to the north and south (Figure 7a). The main brittle strand of the SJF juxtaposes interbedded andesite, basalt, limestone, and volcaniclastic sediments of the Bonanza Group (Wrangellia) to the north,

against friable schist of the Leech River Complex (Pacific Rim terrane) to the south. Moderately north-dipping, west-striking foliation characterizes the schist immediately south of the SJF (Figure 7a). Aside from minor folding of the schist, no post-foliation ductile deformation was observed at Site IV. In addition, unlike the sites to the west, a separate generation of normal faulting was not observed at this location. However, similar to Site II, a separate and different generation of reverse faulting is observed north of the SJF in rocks of the Wrangellia terrane.

The main terrane-juxtaposing strand of the SJF is visible in outcrop at one location (Figure 7a), where it is a ∼10 m-wide left-lateral shear zone separating Bonanza Group volcanic rocks and the Leech River Complex schist (Figures 7b and 7c). This fault has a ∼1 m-wide fault core that exhibits a scaly fabric consisting of anastomosing shear surfaces coated with chlorite. No obvious slickenline orientations are visible in the fault core. In the damage zone immediately north of the scaly fault core, several ∼0.1–1 m-wide zones of intense deformation, marked by increased fracture and slip surface density, occur at a m-scale spacing. The rocks in between the zones of intense deformation also exhibit fractures and slip surfaces at a lower density than observed in the fault core. Kinematic inversion of 8 (out of 9) slickenline orientations from the damage zone, excluding the one right-lateral fault plane, is consistent with left-lateral slip on a steeply south-dipping, east-striking fault plane (bottom left stereonet, Figure 7a).

Several <1 m-wide left-lateral faults branch off the SJF at Site IV. To the north of the SJF in the Bonanza Group volcanic rocks, these faults are steeply dipping and strike at an angle of <45° to the contact fault. Major faults have ∼1−2 cm-thick anastomosing layers of clay to fine sand gouge within the fault core. Their damage zones consist of fractures and slip surfaces with calcite, epidote, quartz, and chlorite slickenfibers (e.g., Figures 7d and 7e). At the eastern extent of Site IV, kinematic analysis of one of the faults branching north from the SJF indicates left-lateral slip (far right stereonet, Figure 7a). To the south in the Leech River Complex, drag folding (Figure 7f) also indicates left-lateral shear on a northeast-striking fault cross-cutting schist foliation.

A ∼50 m-wide south-dipping reverse fault zone is located ∼600 m north of the SJF in the Bonanza Group volcanic rocks within the Wrangellia terrane (Figure 7a). The fault zone consists of brecciated volcanic rocks with pervasive calcite and quartz veins, and meter-thick zones of cataclasite consisting of pulverized volcanic rocks, calcite, and quartz. Six slickenline orientations from within the fault zone indicate north-verging reverse slip (top-middle stereonet, Figure 7a).

To assess the overall kinematics of the SJF at Site IV, we incorporated all of the fault plane and slickenline measurements ($n = 71$) from within 500 m of the main lithological contact fault into a kinematic inversion model. This selection excluded fault plane and slickenline orientations from the reverse fault ∼600 m north of the SJF, as we interpret this structure to belong to a different generation of faulting due to its incompatible kinematic axes and its location north of the main SJF fault zone. The selected fault planes are predominantly moderately to steeply south-dipping and strike east-northeast. Kinematic inversion of 51 compatible measurements (out of 71) suggests that these faults accommodated left-lateral slip (Table 2; stereonets at top left, Figure 7a).

5.2.5. Site V

Site V spans the ∼30 km of the SJF that is east of the Survey Mountain fault. This portion of the SJF is not terrane-juxtaposing, and instead offsets different units of Wrangellia (Figure 2). The SJF is expressed as a single fault strand in the western half of Site V, branching into two strands in the eastern half of Site V (Figure 8). The northern southwest-striking branch of the SJF projects northeast toward the Nanaimo Group sediments where it is obscured by Quaternary cover. Just east of this fault branch, we mapped a ∼700 m by ∼300 m-wide abandoned limestone quarry exposing Paleozoic volcaniclastic rocks and limestone capped by basalt. In the western portion of Site V, our observations were limited to a few outcrops along the SJF (Figure 8).

The quarry at Site V exposes a ∼30 m-wide, steeply north-dipping, west-southwest-striking fault zone that cross-cuts limestone and fine-grained sediments. The main fault zone in the quarry has several subvertical ∼1−2 m-wide faults that exhibit dark green to black scaly fabric formed from chlorite mineralization. Fault gouge in these meter-wide faults also contains pulverized ankerite and calcite. Narrower fault cores (<30 cm) within the larger faults and planar fractures have calcite slickenfibers. Kinematic inversion of 21 fault slickenlines measured from within the main shear zone indicates reverse slip accommodating north-south shortening (Figure 8).

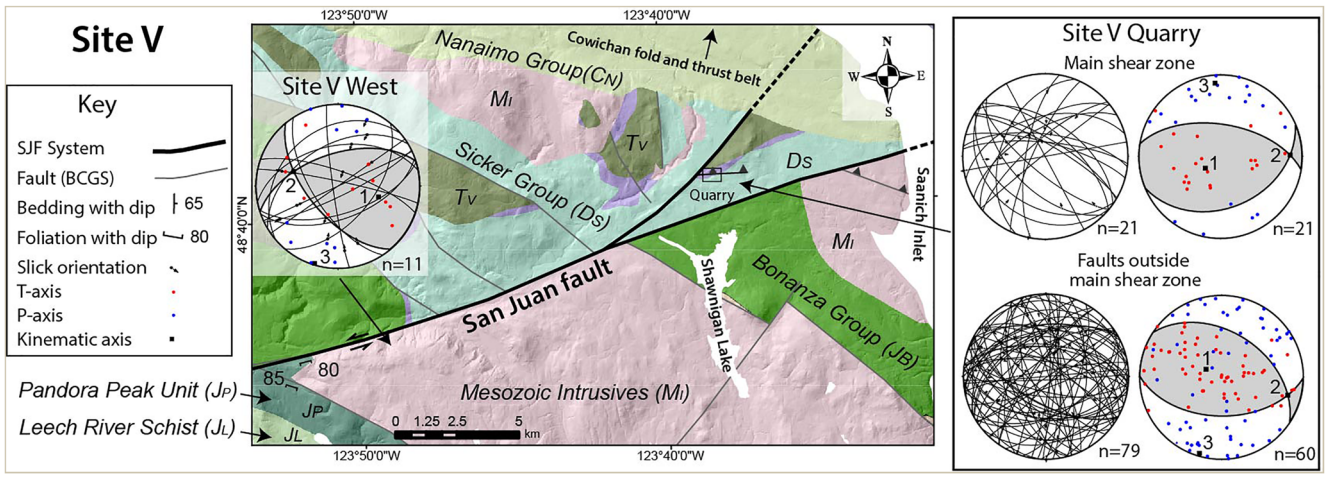

Figure 8. Geologic map of Site V along with stereonet projections showing fault planes, slickenlines, and kinematic inversions using *n* compatible measurements. Tabulated kinematic axes data is shown in Table 2. The Site V quarry is located near a southwest-striking fault strand oblique to and north of the main SJF. Site V west is located on the main strand of the SJF. Geologic legend is the same as Figure 2. Detailed geologic map of the Site V quarry and fault photos are shown in Figure S9 in Supporting Information S1.

Outside of the west-southwest-striking main fault zone faults vary from narrow (~1 cm-wide) planar structures with little cataclasite, to ~0.5–2 m-thick faults containing fault breccia and gouge. The majority of fault slickenlines (n = 60) also indicate reverse slip accommodating ~ north-south shortening, suggesting these faults are related to the main fault zone (Table 2; Figure 8). From these kinematic inversions, we infer that the main west-southwest-striking fault zone at the Site V quarry is a reverse fault that is parallel and related to the Cowichan fold and thrust belt.

Approximately 16 km southwest of the quarry at Site V, observations of brittle faulting along the main strand of the SJF indicate oblique left-lateral slip. Kinematic inversions of 11 compatible (of 13 total) slickenline orientations show north-south maximum horizontal shortening accommodated by left-lateral slip on a steeply north-dipping west-striking fault plane (Table 2; Figure 8).

6. Discussion

6.1. Left-Lateral Brittle Slip on the SJF

Our structural analyses and geologic mapping indicate the brittle SJF was a major structure that primarily accommodated left-lateral slip or left-oblique with a reverse component of slip, on an east-to northeast-striking, steeply dipping fault. On Figure 9a we show that at each site along the entire ~80 km length of the SJF, there is a population of faults with a pseudo fault-plane solution that shares common south-southwest-north-northeast maximum shortening axes consistent with left-lateral slip (Kinematic axis 3, Table 2). Left-lateral faults with similar maximum shortening axes are also observed on northeast-striking faults branching southwards from the SJF at Site III (Figure 6b). At Site IV, we directly observe the fault contact between Wrangellia and the Pacific Rim terrane to have left-lateral kinematic indicators (Figure 7b). The observation that the southwestern boundary of the Wrangellia terrane is apparently offset by ~60 km across the SJF (Figure 2; DeBari et al., 1999; Muller, 1977), combined with our observations of left-lateral fault kinematics, shows the SJF was a major structure that accommodated significant displacement.

The kinematics of many of the minor faults along the SJF are also consistent with regional left-lateral shear along the main strand of the fault. North-northwest to west striking reverse faults within ~1 km of the SJF at Site I (Figure 3), and ~500 m of the SJF at Site V (Figure 8), are kinematically compatible with the northeast-southwest maximum shortening direction observed along the length of the SJF (Figure 9a). Similarly, right-lateral faults that cross-cut the SJF at Sites I and II (Figure 9a) also exhibit similar maximum shortening axes to the left-lateral fault plane solutions at Sites I and II. These right-lateral faults are oriented <45° from the main strand of the SJF, not the ~75° typical of an antithetic fault (e.g., Fossen, 2016), and may suggest reactivation of older, northwest-southeast

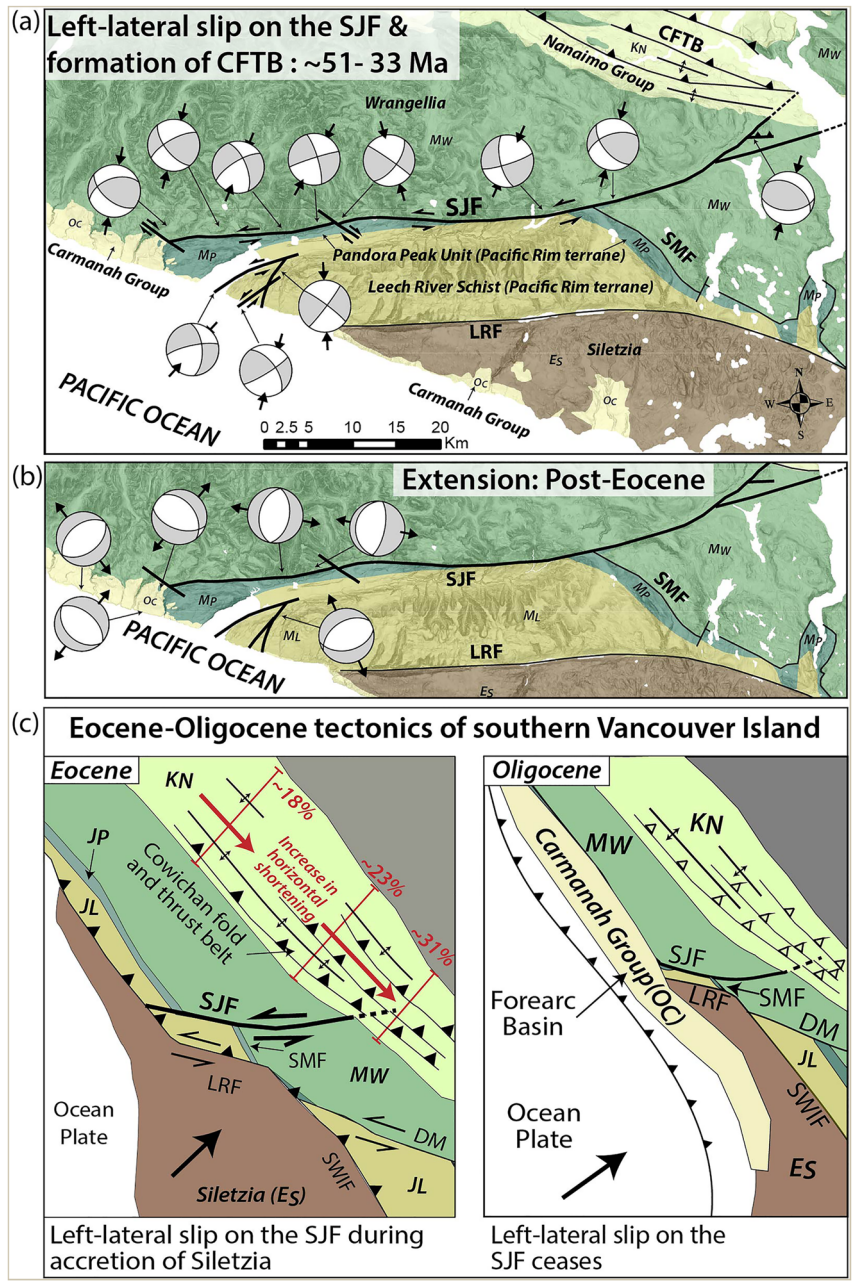

Figure 9. (a and b) Terrane map of southern Vancouver Island showing two separate deformation events with pseudo fault plane solutions. (a) ~51−33 Ma left-lateral and oblique thrust faulting along the San Juan fault (SJF) that is compatible with north-northeast south-southwest shortening accommodated by the Cowichan fold and thrust belt (CFTB). Arrows on fault plane solutions show the maximum shortening axis (minimum extension: kinematic axis 3, Table 2). (b) Post-Eocene northwest-southeast and southwest-northeast extension accommodated by normal faults cross-cutting the Carmanah Group and the underlying Pacific Rim terrane. Leech River fault (LRF) and Survey Mountain fault (SMF) shown for reference. Arrows on fault plane solutions show the maximum extension axis (kinematic axis 1, Table 2). (c) Our proposed Eocene-Oligocene tectonic evolution of northern Cascadia. Active fault kinematics are shown for each time period; inactive faults either have no kinematics shown, or have hollow teeth on the thrust hanging wall. **Eocene:** Accretion of Siletzia along the LRF (e.g., Clowes et al., 1987) and the SWIF (e.g., Johnson et al., 1996) results in left-lateral slip on the SJF, and southeast-increasing horizontal shortening accommodated by the Cowichan fold and thrust belt. **Oligocene:** Left-lateral slip on the SJF has ceased, subduction has stepped outboard of Siletzia, and marine sediments of the Carmanah Group are deposited in a forearc basin. Geologic legend is the same as Figure 1.

trending margin-parallel structures. These faults cross-cut and offset the main strand of the SJF by up to 1 km at Site I, and 500 m at Site II, suggesting that if they are related, they developed in the later stages of deformation along the SJF.

There are two groups of faults where the kinematics derived from slickensides are not consistent with left-lateral oblique-slip on the SJF: thrust fault populations at Sites II and IV suggestive of northwest-southeast maximum shortening (Figures 6a and 7a), and the numerous normal faults observed at Sites I, II, and III that suggest extension. However, the anomalous deformation observed in both groups of faults is spatially restricted and did not affect the rocks along the entire length of the SJF. Thrust faulting at Sites II and IV is only observed north of the SJF in Wrangellia (Figures 6a and 7a). Similarly, the normal fault populations are only observed at the western 15 km extent of the SJF (Figure 9b). Therefore, we interpret these reverse and normal faults to represent separate generations of deformation unrelated to the significant left-lateral slip we document on the SJF.

6.2. Timing of Left-Lateral Slip on the SJF

The observation of the Carmanah Group non-conformably overlying the SJF at Site I constrains the minimum age of slip on the SJF. First, we found no evidence of significant strike-slip or reverse faulting in the Carmanah Group sediments above the location of the SJF in the basement terranes. Furthermore, the southwest-dipping basal unconformity of the Carmanah Group at Sites I and III occurs at sea level on either side of the inlet (Port San Juan, Figures 2, 3, and 6), which suggests no major strike-slip or dip-slip offset of the elevation of the basal non-conformity has occurred immediately northwest of the town of Port Renfrew (Figure 2). The lack of strike-slip faulting within the Carmanah Group suggests that left-lateral strike-slip faulting on the SJF ceased before the deposition of these sediments (as suggested by Rusmore & Cowan, 1985).

Our Sr isotope date and previous estimates of the depositional age of the Carmanah Group at Site I therefore constrains the minimum age of brittle left-lateral slip along the SJF to ~33 Ma (Figure 4; Table 1). We obtained this age from a sample collected from sediments <60 m above the basal non-conformity of the Carmanah Group. If we assume that the continental shelf setting associated with the rocks had a high sedimentation rate typical of forearc basin settings (e.g., greater than 500 m/Myr, Ito, 1992; G. F. Moore et al., 2015), the derived Oligocene age could closely represent the time when deposition of the Carmanah Group commenced. A late Eocene–early Oligocene age for the section of Carmanah Group sediments at Site I is further supported by Eocene-Oligocene ages from other Carmanah Group sites, with similar lithologies, on the west coast of Vancouver Island (Cameron, 1980; Johns et al., 2012; Narayan et al., 2005; Prothero et al., 2008; Tiffin et al., 1972).

Although the available data do not provide direct constraints on the maximum age for brittle left-lateral slip on the SJF, cross-cutting relationships with previously dated units and metamorphic fabrics suggest that the earliest the brittle SJF was active was the early Eocene. Brittle left-lateral faulting along the SJF cross-cuts metamorphic schistose fabric in the Leech River Complex (e.g., Figure 7f), and this schistose fabric has been dated to either 51 Ma (Groome et al., 2003) or 41−39 Ma (Fairchild & Cowan, 1982). We favor the metamorphic age from Groome et al. (2003), as it is based on the ages of the Walker Creek intrusions, interpreted to result from anatexis of the Leech River Complex sediments during peak metamorphic conditions (greenschist to amphibolite, high-T low-P conditions). In contrast, the Fairchild and Cowan (1982) metamorphic ages are based on K-Ar cooling ages and may not be indicative of peak metamorphism. The ~51 Ma Walker Creek intrusions are also cross-cut by left-lateral faulting at Site III (Figure 6), which we interpret is related to left-lateral slip on the SJF.

The cross-cutting relations described above provide a bracket on the timing of the brittle portion of deformation; the maximum age of ductile deformation is less constrained. We speculate that early, apparent left-lateral ductile shear within proximity to the SJF at Sites I and II was either contemporaneous with or predated the development of schistose fabric in the Leech River Complex. The schistose fabric (Figures 6 and 7a), and folding of this fabric, are both consistent with a south-southwest north-northeast shortening direction (Figure 6c; Fairchild & Cowan, 1982). This shortening direction is roughly compatible with maximum shortening accommodated by left-lateral slip on the SJF (Figure 9) and ductile deformation of the Leech River Complex and the Pandora Peak unit may have evolved into brittle deformation during exhumation. However, ductile deformation in the Pandora Peak unit could also predate metamorphism of the Leech River Complex as peak metamorphism occurred significantly earlier (99–83 Ma), and the pressure-temperature conditions of the Pandora Peak are different (Rusmore & Cowan, 1985). These observations instead suggest that ductile deformation in the Pandora Peak unit may be

related to earlier accretion of the Pacific Rim terrane to Wrangellia. Therefore, while we constrain the maximum age of brittle deformation to ∼51 Ma, we acknowledge that ductile deformation on the system may have begun earlier.

6.3. Left-Lateral Slip on the SJF During Accretion of Siletzia

The overlap in timing between left-lateral brittle faulting along the SJF (∼51−33 Ma) and the accretion of Siletzia (51–42.5 Ma,Eddy et al., 2016; England et al., 1997; Evans & Ristow, 1994; Groome et al., 2003; Johnson, 1984b; Miller et al., 2016; Wells et al., 2014) suggests that fault slip was related to this accretion (Figure 9c). The accretion age of Siletzia on Vancouver Island is based on sedimentary sequence analyses and structural mapping in western Washington State, and exhumation ages from rocks in the Leech River Complex and sediments deformed by the Cowichan fold and thrust belt. Eddy et al. (2016) show that changes in paleoflow directions and increased sedimentation rates in the Swauk basin, east of Siletzia, occurred between 51.3 and 49.9 Ma and were likely due to accretion of Siletzia. Additionally, northwest-southeast trending, upright folding of the Swauk basin sediments and nearby Skagit gneiss complex that is constrained to between 51 and 49 Ma (Miller et al., 2016) is consistent with the accretion of Siletzia at this time. To the northwest, 50 Ma exhumation ages from apatite fission track dating of sediments in the Cowichan fold and thrust belt (Currie & Grist, 1996; England et al., 1997; Evans & Ristow, 1994; Johnson, 1984b) have been linked to deformation resulting from accretion of Siletzia. Finally, Ar^{40}/Ar^{39} cooling ages of muscovite and biotite from the Leech River Complex, located in between Siletzia and the Cowichan fold and thrust belt, indicate cooling interpreted to result from accretion-related exhumation between 51 and 42.5 Ma (Groome et al., 2003). These ages all point to accretion of Siletzia occurring during, and most likely near the beginning of, our inferred ∼51−33 Ma time bracket for left-lateral slip on the SJF.

In addition to the overlap in timing, left-lateral slip or left-oblique with a reverse component of slip are also consistent with patterns of deformation resulting from the collision of Siletzia observed by previous workers (Eddy et al., 2017; England & Calon, 1991; Johnson et al., 1996; Johnston & Acton, 2003; Massey, 1986; McCrory & Wilson, 2013; Wells et al., 2014). In the Eocene Cowichan fold and thrust belt northeast of the SJF, we assume southwest-northeast horizontal shortening perpendicular to the strike of the folds and thrust faults mapped in the Nanaimo Group sediments (Figure 9a; England & Calon, 1991). The maximum horizontal shortening axis associated with left-lateral slip on the SJF is subparallel to the shortening direction associated with the Cowichan fold and thrust belt (Figures 9a and 9c). This observation, along with the observation that both structures were active in the Eocene, suggests that the SJF and Cowichan fold and thrust belt may be kinematically linked, and are both related to the Eocene collision of Siletzia.

We infer that because the SJF was active at the same time as the Cowichan fold and thrust belt, Eocene left-lateral slip could also deform the Cretaceous Nanaimo Group sediments (Figure 9c). England and Calon (1991) suggest the SJF offsets and soles into the frontal northwest-striking reverse faults of the Cowichan fold and thrust belt, consistent with both structures being active at the same time. This geometry also explains the significantly lesser inferred offset of the Nanaimo Group sediments and Cowichan fold and thrust belt, compared to the ∼60 km of apparent offset of Wrangellia (Figures 2 and 9c). However, outcrops that could further determine these relationships are obscured by cover and the Saanich Inlet (Figure 2), and therefore the exact structural relations between the Nanaimo Group, the Cowichan fold and thrust belt, and the SJF are still unclear.

If left-lateral slip on the SJF is related to collision of Siletzia, we suggest that it could have helped accommodate the along-strike gradient in minimum shortening documented in the Cowichan fold and thrust belt (18% to ∼31% over ∼60 km toward the southeast, Figure 9c; England & Calon, 1991; Johnston & Acton, 2003), when both were active in the Eocene. We speculate the southeastward increase in shortening may be due to accretion of a thicker or more buoyant portion of Siletzia in the southeast (Washington State) by comparison to the northwest (British Columbia; e.g., Johnston & Acton, 2003). The Eocene eruption of ocean island basalts associated with Siletzia (Massey, 1986; Phillips et al., 2017; Wells et al., 2014), and collision during eruption and shortly thereafter (e.g., England et al., 1997; Timpa et al., 2005; Wells et al., 2014), could have resulted in the subduction of relatively young and buoyant lithosphere, a process that can lead to frontal or basal accretion (K. Vogt & Gerya, 2014). Both basal and frontal accretion involve accretion of oceanic material onto the continental margin and result in significant deformation of the upper crust (K. Vogt & Gerya, 2014). Collision of an isolated portion of more buoyant crust, such as a recently erupted oceanic plateau or an active spreading center, has been shown to cause localized crustal shortening, or indentation, of the overriding plate (e.g., P. R. Vogt et al., 1976; Wallace et al., 2009). The

left-lateral slip along the SJF could have facilitated the Eocene indentation of the oceanic plateau of Siletzia and the associated lateral shortening gradient. Eocene left-lateral slip observed on other similar-striking crustal faults to the south of the SJF, including the Leech River fault (Fairchild & Cowan, 1982) and Devils Mountain fault (Evans & Ristow, 1994; Hayward et al., 2006; Johnson et al., 2001; Personius et al., 2014), may have also accommodated this crustal shortening gradient due to oceanic plateau collision (Figure 9c).

6.4. Implications for the History of Terrane Amalgamation on Southern Vancouver Island

Our results suggest that although the brittle SJF separates the Pacific Rim terrane from Wrangellia, accretion of the Pacific Rim terrane was not accommodated by brittle left-lateral slip along the fault (e.g., Brandon, 1989b; Johnson, 1984a; MacLeod et al., 1977; Muller, 1977). We speculate that the Pacific Rim terrane was instead accreted to the western margin of Wrangellia along a northwest-southeast trending plate boundary fault that included the Survey Mountain fault (e.g., Rusmore & Cowan, 1985). Rather than accommodating accretion of the Pacific Rim terrane, the brittle SJF was a major strike-slip structure cross-cutting the older Survey Mountain fault, and accommodating upper plate deformation during the Eocene accretion of Siletzia (Figure 9c).

Our interpretation of Eocene left-lateral slip on the SJF suggests that the original Late Cretaceous terrane boundary between the Pacific Rim terrane and Wrangellia (Survey Mountain fault) was offset left-laterally during the Eocene (Figure 9c). The continuation of the Survey Mountain fault could be the northwest-striking West Coast fault which separates the Pacific Rim terrane from Wrangellia along the west coast of Vancouver Island near the towns of Ucluelet and Tofino, northwest of our study area (Brandon, 1989a). The offset of the original Pacific Rim-Wrangellia terrane boundary (Survey Mountain Fault) is consistent with the SJF juxtaposing rocks with different metamorphic assemblages in the Pandora Peak unit and Wrangellia (Rusmore & Cowan, 1985), in addition to the ∼60 km of apparent left-lateral offset of the Wrangellia terrane across the SJF (Figures 2 and 9).

Ductile deformation observed at Sites I and II may represent evidence of earlier (Cretaceous-Paleogene) deformation related to Pacific Rim terrane accretion. However, the observed ductile deformation could be a result of exhumation of a deeper portion of the Eocene SJF brittle structure. The ductile deformation was observed only in the western portions of the SJF, at Sites I and II, in a region where metamorphic mineral assemblages in previous studies have argued for increased post-Eocene exhumation by comparison to the eastern half of the SJF (Fairchild & Cowan, 1982; Rusmore & Cowan, 1985; Timpa et al., 2005). The observed ductile deformation therefore needs further study before its implications can be understood.

6.5. Erosion, Sedimentation and Deformation Post-Dating SJF Left-Lateral Slip: Forearc Basin Processes?

Our observations within the stratigraphy of the Carmanah Group sediments, and post-Eocene deformation at the western end of the SJF, have implications for the regional post-Eocene tectonic setting. We speculate that sedimentation and apparent sea level rise recorded by fining-upwards stratigraphy (Figure 4) may be related to forearc basin formation after the initiation of the modern Cascadia subduction zone by 45–42 Ma (Figure 9c, du Bray & John, 2011; Eddy et al., 2017; Wells et al., 2014). The deposition of a fining-upward sequence of marine sediments above the erosional non-conformity at the base of the Carmanah Group could imply apparent sea level rise throughout the time period of deposition during the late Eocene to early Oligocene. These observations are consistent with fining-upwards sedimentary sequences observed in the late Eocene Escalante Formation northwest along the coast of Vancouver Island (Cameron, 1980; Jeletzky, 1954; Narayan et al., 2005), and to the south in the late Eocene–early Oligocene Makah Formation on the Olympic Peninsula (Snavely et al., 1980).

In addition, the normal faults we observe to cross-cut both the Carmanah Group sediments and rocks of the Pacific Rim terrane (Figure 9b) could be related to regional extension that is commonly documented in forearc basins (e.g., Conin et al., 2012; Regalla et al., 2017; Vannucchi, Ranero, et al., 2003; Von Huene & Suess, 1988; Wang et al., 2012). The normal faults within the Pacific Rim terrane (Sites I–III, Figures 3, 6a, and 6b) have similar kinematic axes to those in the Carmanah Group (Table 2; Figure 9b) and we infer that both are the result of a distinct deformation event that is younger than the Eocene left-lateral slip we observe on the SJF. At Site I on the west coast of Vancouver Island, normal faults at Q1 and Q2 offset thrust and strike-slip faults (Figure 3; Figures S7 in Supporting Information S1), indicating they are the result of post-Eocene deformation that affected the Carmanah Group. At Sites II and III, the kinematic axes derived from kinematic inversions of these normal fault

populations are subparallel to those in the Carmanah Group (Figure 9b). We also only observe significant normal fault populations in the Pacific Rim terrane within ~15 km of the southwest coast of Vancouver Island, proximal to where normal faults are also documented in the Carmanah Group. Because of their location in what we, and previous authors, interpret as a forearc basin, and their orthogonal orientations, we interpret these normal faults could be similar to orthogonal sets of normal faults found in forearc basins along other margins (e.g., Kumano forearc basin, Sacks et al., 2013).

Finally, because we do not observe strike-slip faulting of the Carmanah Group sediments, we consider the right-lateral faults mapped along the western SJF (Sites I and II) do not represent Quaternary deformation that has been recognized elsewhere on southern Vancouver Island. Paleoseismic investigations of the Leech River fault, 10–25 km south of the SJF (Figure 2), indicate that the eastern, northwest-southeast striking segment of this structure has hosted Holocene right-lateral oblique surface rupturing earthquakes (Harrichhausen et al., 2021; Morell et al., 2017, 2018). As the Carmanah Group sediments only overlie the SJF at the western end of the fault, it is possible that only the western SJF may be inactive (Sites I and II), and we cannot rule out active right-lateral faulting at Sites IV and V to the east. Further studies are required to test this hypothesis.

7. Conclusion

Kinematic analyses and geologic mapping show the SJF was a major strike-slip fault that accommodated left-lateral brittle slip. Brittle left-lateral slip along the SJF cross-cuts ~51 Ma metamorphic foliation and magmatic dykes, while marine shelf sediments of the Carmanah Group non-conformably overlie the SJF at the western end of the fault. A Sr isotope date of foraminifers from these sediments suggests their deposition in the late Eocene–early Oligocene, which is consistent with previous age estimates and constrains the timing of left-lateral slip on the SJF to the Eocene. This Eocene left-lateral slip along the SJF is temporally and kinematically consistent with north-northeast-south-southwest shortening during formation of the Cowichan fold and thrust belt and accretion of the Siletzia ocean island plateau. We suggest the SJF, along with a network of crustal faults in northern Cascadia, accommodated a southeastward increase in crustal shortening resulting from accretion of a more buoyant, potentially younger, or thicker, portion of Siletzia south of the SJF. Orthogonal west-northwest trending (coast-parallel) and north-northeast trending (coast-perpendicular) normal faults, that we observe deforming the late Eocene–early Oligocene Carmanah Group sediments, are post-terrane accretion and not related to slip on the SJF.

Data Availability Statement

Additional figures are provided in the Supplementary Material. Tabulated structural data, and Sr isotope data (Harrichhausen et al., 2022) are stored in a data repository that can be accessed at: https://datadryad.org/stash/dataset/doi:10.25349/D9CD03. Topographical data used to create geology maps are from the Canadian Digital Elevation Model Database available at: https://open.canada.ca/data/en/dataset/957782bf-847c-4644-a757-e383c0057995. Stereonet 10.1.6 and FaultKin 8.1.2, used for structural analyses and kinematic inversions, are both available at https://www.rickallmendinger.net/.

Acknowledgments
Funding for this project is provided by National Science Foundation Earth Science (NSF EAR) Grant 1756943 to K. Morell, and NSF EAR Grant 1756834 to C. Regalla. Additionally, N. Harrichhausen was supported by a National Science and Engineering Research Council (NSERC) Post Graduate Scholarship and Geological Society of America (GSA) Graduate Student Research Grant. The authors would like to thank the Pacheedaht First Nation for generously granting access to their land and for their interest in our research; Parks Canada for providing access, allowing for sample collection, and providing logistical support for work in Pacific Rim National Park; and TimberWest Forest Corporation and Island Timberlands for providing land access and logistical support for work on their respective properties. The authors thank M. Johns for helping to collect samples, and for processing, extracting, and identifying foraminifers for Sr isotope analyses; M. Makahnouk for Sr isotope analyses; and E. Humphrey for the scanning electron microscopy images used for foraminifer identification. K. Johnson, S. Mracek, C. Anderson, S. Dyer, and C. Green all assisted in field work and provided valuable input on our research. C. Goldblatt, and S. Citerneschi and L. Syme Citerneschi generously provided accommodation for N. Harrichhausen and K. Morell during multiple field campaigns. The authors also thank E. Nissen and the University of Victoria for logistical support and engaging discussions about regional tectonics. Thoughtful reviews and comments from B. Miller, E. Schermer, and editors M. Rusmore and R. Cecil were of great help and well appreciated.

References

Allmendinger, R. W., Cardozo, N., & Fisher, D. M. (2011). *Structural geology algorithms: Vectors and tensors*. Cambridge University Press.

Allmendinger, R. W., Gephart, J. W., & Marrett, R. A. (1989). Notes on fault slip analysis. *Geological Society of America Short Course on Quantitative Interpretation of Joints and Faults*, *66*, 1.

Betka, P., Klepeis, K., & Mosher, S. (2016). Fault kinematics of the Magallanes-Fagnano fault system, southern Chile; an example of diffuse strain and sinistral transtension along a continental transform margin. *Journal of Structural Geology*, *85*, 130–153. https://doi.org/10.1016/j.jsg.2016.02.001

Bird, P. (2003). An updated digital model of plate boundaries. *Geochemistry, Geophysics, Geosystems*, *4*(3). https://doi.org/10.1029/2001GC000252

Bradbury, K. K., Evans, J. P., Chester, J. S., Chester, F. M., & Kirschner, D. L. (2011). Lithology and internal structure of the San Andreas fault at depth based on characterization of Phase 3 whole-rock core in the San Andreas Fault Observatory at Depth (SAFOD) borehole. *Earth and Planetary Science Letters*, *310*(1–2), 131–144. https://doi.org/10.1016/j.epsl.2011.07.020

Brandon, M. T. (1989a). Deformational styles in a sequence of olistostromal mélanges, Pacific Rim Complex, western Vancouver Island, Canada. *The Geological Society of America Bulletin*, *101*(12), 1520–1542. https://doi.org/10.1130/0016-7606(1989)101<1520:dsiaso>2.3.co;2

Brandon, M. T. (1989b). Origin of igneous rocks associated with melanges of the Pacific Rim Complex, western Vancouver Island, Canada. *Tectonics*, *8*(6), 1115–1136. https://doi.org/10.1029/tc008i006p01115

Brandon, M. T., Orchard, M. J., Parrish, R. R., Sutherland Brown, A., & Yorath, C. J. (1986). Fossil ages and isotopic dates from the Paleozoic Sicker Group and associated intrusive rocks, Vancouver Island, British Columbia. In *Current research, part A* (pp. 683–696). Geological Survey of Canada. https://doi.org/10.4095/120440

Brandon, M. T., Roden-Tice, M. K., & Garver, J. I. (1998). Late Cenozoic exhumation of the Cascadia accretionary wedge in the Olympic Mountains, northwest Washington State. *The Geological Society of America Bulletin*, *110*(8), 985–1009. https://doi.org/10.1130/0016-7606(1998)110<0985:lceotc>2.3.co;2

Calvert, A. J. (1996). Seismic reflection constraints on imbrication and underplating of the northern Cascadia convergent margin. *Canadian Journal of Earth Sciences*, *33*(9), 1294–1307. https://doi.org/10.1139/e96-098

Cameron, B. E. B. (1980). *Biostratigraphy and depositional environment of the Escalante and Hesquiat formations (early Tertiary) of the Nootka Sound area, Vancouver Island, British Columbia* (pp. 1–28). Geological Survey of Canada Paper. 78-9

Cardozo, N., & Allmendinger, R. W. (2013). Spherical projections with OSXStereonet. *Computers & Geosciences*, *51*, 193–205. https://doi.org/10.1016/j.cageo.2012.07.021

Clapp, C. H., & Cooke, H. C. (1917). *Sooke and Duncan Map-areas, Vancouver Island* (Vol. 96, p. 445). Geological Survey of Canada, Memoir.

Clowes, R. M., Brandon, M. T., Green, A. G., Yorath, C. J., Brown, A. S., Kanasewich, E. R., & Spencer, C. (1987). LITHOPROBE—southern Vancouver Island: Cenozoic subduction complex imaged by deep seismic reflections. *Canadian Journal of Earth Sciences*, *24*(1), 31–51. https://doi.org/10.1139/e87-004

Conin, M., Henry, P., Godard, V., & Bourlange, S. (2012). Splay fault slip in a subduction margin, a new model of evolution. *Earth and Planetary Science Letters*, *341*, 170–175. https://doi.org/10.1016/j.epsl.2012.06.003

Cowan, D. S. (1985). Structural styles in Mesozoic and Cenozoic mélanges in the western Cordillera of North America. *The Geological Society of America Bulletin*, *96*(4), 451–462. https://doi.org/10.1130/0016-7606(1985)96<451:ssimac>2.0.co;2

Cui, Y., Miller, D., Schiarizza, P., & Diakow, L. (2017). British Columbia digital geology. *British Columbia Ministry of Energy, Mines and Petroleum Resources, British Columbia Geological Survey Open File*, *8*(9). Retrieved from https://www2.gov.bc.ca/gov/content/industry/mineral-exploration-mining/british-columbia-geological-survey/geology/bcdigitalgeology

Currie, L., & Grist, A. (1996). *Diachronous low-temperature Paleogene cooling of the Alberni Inlet area, southern Vancouver Island, British Columbia: Evidence from apatite fission track analyses* (pp. 119–125). Geological Survey of Canada Current Research, 1996.

Davis, G. A., Monger, J., & Burchfiel, B. (n.d). Mesozoic construction of the Cordilleran "collage", central British Columbia to central California. In D. G. Howell, & K. A. McDougall (Eds.), *Mesozoic Paleogeography of the Western United States, Pacific Coast Paleogeography Symposium 2: Los Angeles, California, Pacific Section, Society of Economic Paleontologists and Mineralogists (SEPM)* (pp. 1–32).

DeBari, S. M., Anderson, R. G., & Mortensen, J. K. (1999). Correlation among lower to upper crustal components in an island arc: The Jurassic Bonanza arc, Vancouver Island, Canada. *Canadian Journal of Earth Sciences*, *36*(8), 1371–1413. https://doi.org/10.1139/e99-029

Dickinson, W. R. (2004). Evolution of the North American Cordillera. *Annual Review of Earth and Planetary Sciences*, *32*, 13–45. https://doi.org/10.1146/annurev.earth.32.101802.120257

Doblas, M. (1998). Slickenside kinematic indicators. *Tectonophysics*, *295*(1–2), 187–197. https://doi.org/10.1016/s0040-1951(98)00120-6

Donaghy, E. E., Umhoefer, P. J., Eddy, M. P., Miller, R. B., & LaCasse, T. (2021). Stratigraphy, age, and provenance of the Eocene Chumstick basin, Washington Cascades; implications for paleogeography, regional tectonics, and development of strike-slip basins. *GSA Bulletin*, *133*(11–12), 2418–2438. https://doi.org/10.1130/b35738.1

du Bray, E. A., & John, D. A. (2011). Petrologic, tectonic, and metallogenic evolution of the Ancestral Cascades magmatic arc, Washington, Oregon, and northern California. *Geosphere*, *7*(5), 1102–1133. https://doi.org/10.1130/ges00669.1

Eddy, M. P., Bowring, S. A., Umhoefer, P. J., Miller, R. B., McLean, N. M., & Donaghy, E. E. (2016). High-resolution temporal and stratigraphic record of Siletzia's accretion and triple junction migration from nonmarine sedimentary basins in central and western Washington. *GSA Bulletin*, *128*(3–4), 425–441. https://doi.org/10.1130/B31335.1

Eddy, M. P., Clark, K. P., & Polenz, M. (2017). Age and volcanic stratigraphy of the Eocene Siletzia oceanic plateau in Washington and on Vancouver Island. *Lithosphere*, *9*(4), 652–664. https://doi.org/10.1130/l650.1

England, T. D. J., & Calon, T. J. (1991). The Cowichan fold and thrust system, Vancouver Island, southwestern British Columbia. *The Geological Society of America Bulletin*, *103*(3), 336–362. https://doi.org/10.1130/0016-7606(1991)103<0336:tcfats>2.3.co;2

England, T. D. J., Currie, L. D., Massey, N. W. D., Roden-Tice, M. K., & Miller, D. S. (1997). Apatite fission-track dating of the Cowichan fold and thrust system, southern Vancouver Island, British Columbia. *Canadian Journal of Earth Sciences*, *34*(5), 635–645. https://doi.org/10.1139/e17-050

Evans, J. E., & Ristow, R. J., Jr. (1994). Depositional history of the southeastern outcrop belt of the Chuckanut Formation: Implications for the Darrington–Devil's Mountain and Straight Creek fault zones, Washington (USA). *Canadian Journal of Earth Sciences*, *31*(12), 1727–1743. https://doi.org/10.1139/e94-154

Fagereng, Å., Remitti, F., & Sibson, R. H. (2011). Incrementally developed slickenfibers—Geological record of repeating low stress-drop seismic events? *Tectonophysics*, *510*(3–4), 381–386. https://doi.org/10.1016/j.tecto.2011.08.015

Fairchild, L. H., & Cowan, D. S. (1982). Structure, petrology, and tectonic history of the Leech River complex northwest of Victoria, Vancouver Island. *Canadian Journal of Earth Sciences*, *19*(9), 1817–1835. https://doi.org/10.1139/e82-161

Fossen, H. (2016). *Structural geology*. Cambridge University Press.

Garver, J. I., & Brandon, M. T. (1994). Erosional denudation of the British Columbia Coast Ranges as determined from fission-track ages of detrital zircon from the Tofino basin, Olympic Peninsula, Washington. *The Geological Society of America Bulletin*, *106*(11), 1398–1412. https://doi.org/10.1130/0016-7606(1994)106<1398:edotbc>2.3.co;2

Groome, W. G., Thorkelson, D. J., Friedman, R. M., Mortensen, J. K., Massey, N. W. D., Marshall, D. D., & Layer, P. W. (2003). Magmatic and tectonic history of the Leech River Complex, Vancouver Island, British Columbia: Evidence for ridge-trench intersection and accretion of the Crescent Terrane. In *Magmatic and tectonic history of the Leech River Complex, Vancouver Island, British Columbia: Evidence for ridge-trench intersection and accretion of the Crescent Terrane* (pp. 327–354). Special Papers-Geological Society of America. https://doi.org/10.1130/0-8137-2371-x.327

Groshong, R. H., Jr. (2006). *Three-dimesional structural geology* (2nd ed.), Springer. https://doi.org/10.1007/978-3-540-31055-6

Harrichhausen, N., Morell, K. D., Regalla, C., Bennett, S. E., Leonard, L. J., Lynch, E. M., & Nissen, E. (2021). Paleoseismic trenching reveals Late Quaternary kinematics of the Leech River fault: Implications for forearc strain accumulation in northern Cascadia. *Bulletin of the Seismological Society of America*, *111*(2), 1110–1138. https://doi.org/10.1785/0120200204

Harrichhausen, N., Morell, K. D., Regalla, C., Lynch, E. M., & Leonard, L. J. (2022). Eocene Terrane Accretion in Northern Cascadia Recorded by Brittle Left-lateral Slip on the San Juan Fault [Dataset]. Dryad. https://datadryad.org/stash/dataset/doi:10.25349/D9CD03

Hasebe, N., & Tagami, T. (2001). Exhumation of an accretionary prism—Results from fission track thermochronology of the Shimanto Belt, southwest Japan. *Tectonophysics*, *331*(3), 247–267. https://doi.org/10.1016/s0040-1951(00)00282-1

Hayward, N., Nedimović, M. R., Cleary, M., & Calvert, A. J. (2006). Structural variation along the Devil's Mountain fault zone, northwestern Washington. *Canadian Journal of Earth Sciences*, *43*(4), 433–446. https://doi.org/10.1139/e06-002

Hyndman, R. D., Yorath, C. J., Clowes, R. M., & Davis, E. E. (1990). The northern Cascadia subduction zone at Vancouver Island: Seismic structure and tectonic history. *Canadian Journal of Earth Sciences*, *27*(3), 313–329. https://doi.org/10.1139/e90-030

Ito, M. (1992). High-frequency depositional sequences of the upper part of the Kazusa Group, a middle Pleistocene forearc basin fill in Boso Peninsula, Japan. *Sedimentary Geology*, *76*(3–4), 155–175. https://doi.org/10.1016/0037-0738(92)90081-2

Jeletzky, J. A. (1954). *Tertiary rocks of the Hesquiat-Nootka area, West Coast of Vancouver Island, British Columbia (Tech. Rep. No. 53)*. Geological Survey of Canada. https://doi.org/10.4095/101327

Johns, M. J., Trotter, J. A., Barnes, C. R., & Narayan, Y. R. (2012). Biostratigraphic, strontium isotopic, and geologic constraints on the landward movement and fragmentation of terranes within the Tofino basin, British Columbia. *Canadian Journal of Earth Sciences*, *49*(7), 819–856. https://doi.org/10.1139/e2012-032

Johnson, S. Y. (1984a). Evidence for a margin-truncating transcurrent fault (pre-late Eocene) in western Washington. *Geology*, *12*(9), 538–541. https://doi.org/10.1130/0091-7613(1984)12<538:efamtf>2.0.co;2

Johnson, S. Y. (1984b). Stratigraphy, age, and paleogeography of the Eocene Chuckanut Formation, northwest Washington. *Canadian Journal of Earth Sciences*, *21*(1), 92–106. https://doi.org/10.1139/e84-010

Johnson, S. Y., Dadisman, S. V., Mosher, D. C., Blakely, R. J., & Childs, J. R. (2001). *Active tectonics of the Devils Mountain Fault and related structures, northern Puget Lowland and eastern Strait of Juan de Fuca region, Pacific Northwest*. U.S. Geological Survey Professional Paper (1643). (2 plates). https://doi.org/10.3133/pp1643

Johnson, S. Y., Potter, C. J., Miller, J. J., Armentrout, J. M., Finn, C., & Weaver, C. S. (1996). The southern Whidbey Island fault: An active structure in the Puget Lowland, Washington. *The Geological Society of America Bulletin*, *108*(3), 334–354. https://doi.org/10.1130/0016-7606(1996)108<0334:tswifa>2.3.co;2

Johnston, S. T., & Acton, S. (2003). The Eocene Southern Vancouver Island Orocline a response to seamount accretion and the cause of fold-and-thrust belt and extensional basin formation. *Tectonophysics*, *365*(1), 165–183. https://doi.org/10.1016/s0040-1951(03)00021-0

Kant, L. B., Tepper, J. H., Eddy, M. P., & Nelson, B. K. (2018). Eocene basalt of Summit Creek: Slab breakoff magmatism in the central Washington Cascades, USA. *Lithosphere*, *10*(6), 792–805. https://doi.org/10.1130/l731.1

Kirkpatrick, J. D., Rowe, C. D., Ujiie, K., Moore, J. C., Regalla, C., Remitti, F., et al. (2015). Structure and lithology of the Japan Trench subduction plate boundary fault. *Tectonics*, *34*(1), 53–69. https://doi.org/10.1002/2014tc003695

MacLeod, N. S., Tiffin, D. L., Snavely, P. D., Jr., & Currie, R. G. (1977). Geologic interpretation of magnetic and gravity anomalies in the Strait of Juan de Fuca, U.S.-Canada. *Canadian Journal of Earth Sciences*, *14*(2), 223–238. https://doi.org/10.1139/e77-024

Marrett, R., & Allmendinger, R. W. (1990). Kinematic analysis of fault-slip data. *Journal of Structural Geology*, *12*(8), 973–986. https://doi.org/10.1016/0191-8141(90)90093-e

Marrett, R., & Allmendinger, R. W. (1991). Estimates of strain due to brittle faulting: Sampling of fault populations. *Journal of Structural Geology*, *13*(6), 735–738. https://doi.org/10.1016/0191-8141(91)90034-g

Massey, N. W. D. (1986). Metchosin igneous complex, southern Vancouver Island: Ophiolite stratigraphy developed in an emergent island setting. *Geology*, *14*(7), 602–605. https://doi.org/10.1130/0091-7613(1986)14<602:micsvi>2.0.co;2

McArthur, J., Howarth, R., Shields, G., & Zhou, Y. (2020). Chapter 7—Stronitum isotope stratigraphy. In F. M. Gradstein, J. G. Ogg, M. D. Schmitz, & G. M. Ogg (Eds.), *Geologic time scale 2020* (Vol. 1, pp. 211–238). Elsevier. https://doi.org/10.1016/b978-0-12-824360-2.00007-3

McCrory, P. A., & Wilson, D. S. (2013). A kinematic model for the formation of the Siletz-Crescent forearc terrane by capture of coherent fragments of the Farallon and Resurrection plates. *Tectonics*, *32*(3), 718–736. https://doi.org/10.1002/tect.20045

Menant, A., Angiboust, S., Gerya, T., Lacassin, R., Simoes, M., & Grandin, R. (2020). Transient stripping of subducting slabs controls periodic forearc uplift. *Nature Communications*, *11*(1), 1–10. https://doi.org/10.1038/s41467-020-15580-7

Miller, R. B., Bryant, K. I., Doran, B., Eddy, M. P., Raviola, F. P., Sylva, N., & Umhoefer, P. J. (2022). Eocene dike orientations across the Washington Cascades in response to a major strike-slip faulting episode and ridge-trench interaction. *Geosphere*, *18*(2), 697–725. https://doi.org/10.1130/ges02387.1

Miller, R. B., Gordon, S. M., Bowring, S., Doran, B., McLean, N., Michels, Z., et al. (2016). Linking deep and shallow crustal processes during regional transtension in an exhumed continental arc, North Cascades, northwestern Cordillera (USA). *Geosphere*, *12*(3), 900–924. https://doi.org/10.1130/ges01262.1

Monger, J. W. H. (1977). Upper Paleozoic rocks of the western Canadian Cordillera and their bearing on Cordilleran evolution. *Canadian Journal of Earth Sciences*, *14*(8), 1832–1859. https://doi.org/10.1139/e77-156

Monger, J. W. H., & Journeay, J. (1994). Basement geology and tectonic evolution of the Vancouver region. *Geological Survey of Canada Bulletin*, *481*, 3–25. https://doi.org/10.4095/203245

Monger, J. W. H., Price, R. A., & Tempelman-Kluit, D. J. (1982). Tectonic accretion and the origin of the two major metamorphic and plutonic welts in the Canadian Cordillera. *Geology*, *10*(2), 70–75. https://doi.org/10.1130/0091-7613(1982)10<70:taatoo>2.0.co;2

Moore, G. F., Boston, B. B., Strasser, M., Underwood, M. B., & Ratliff, R. A. (2015). Evolution of tectono-sedimentary systems in the Kumano basin, Nankai Trough forearc. *Marine and Petroleum Geology*, *67*, 604–616. https://doi.org/10.1016/j.marpetgeo.2015.05.032

Moore, J. C., Roeske, S., Lundberg, N., Schoonmaker, J., Cowan, D. S., Gonzales, E., & Lucas, S. E. (1986). Scaly fabrics from deep sea drilling project cores from forearcs. In *Structural fabric in deep sea drilling project cores from forearcs* (Vol. 166, pp. 55–73). The Geological Society of America, Inc. https://doi.org/10.1130/mem166-p55

Morell, K. D., Regalla, C., Amos, C., Bennett, S., Leonard, L., Graham, A., et al. (2018). Holocene surface rupture history of an active forearc fault redefines seismic hazard in southwestern British Columbia, Canada. *Geophysical Research Letters*, *45*(21), 11–605. https://doi.org/10.1029/2018gl078711

Morell, K. D., Regalla, C., Leonard, L. J., Amos, C., & Levson, V. (2017). Quaternary rupture of a crustal fault beneath Victoria, British Columbia, Canada. *Geological Society of America Today*, *27*(3–4). https://doi.org/10.1130/gsatg291a.1

Muller, J. E. (1977). Evolution of the Pacific Margin, Vancouver Island, and adjacent regions. *Canadian Journal of Earth Sciences*, *14*(9), 2062–2085. https://doi.org/10.1139/e77-176

Muller, J. E., Cameron, B., & Northcote, K. (1981). *Geology and mineral deposits of the Nootka Sound Map-Area, Vancouver Island, British Columbia* (p. 53). Geological Survey of Canada, Paper 80-16.

Mustard, P. S. (1994). The upper Cretaceous Nanaimo group, Georgia basin. In J. W. H. Monger (Ed.), *Geology and geological hazards of the Vancouver region, southwestern British Columbia* (Vol. 481, pp. 27–95). Geological Survey of Canada, Bulletin. https://doi.org/10.4095/203246

Mustard, P. S., Parrish, R. R., & McNicoll, V. (1995). Provenance of the upper Cretaceous Nanaimo Group, British Columbia: Evidence from U-Pb analyses of detrital zircons. In *Stratigraphic evolution of foreland basins* (pp. 65–76). SEPM (Society for Sedimentary Geology). https://doi.org/10.2110/pec.95.52.0065

Mustoe, G. E., Dillhoff, R. M., & Dillhoff, T. (2007). Geology and paleontology of the early Tertiary Chuckanut Formation. *Field Guides*, *9*, 121–135. https://doi.org/10.1130/2007.fld009(06)

Narayan, Y. R., Barnes, C. R., & Johns, M. J. (2005). Taxonomy and biostratigraphy of Cenozoic foraminifers from Shell Canada wells, Tofino basin, offshore Vancouver Island, British Columbia. *Micropaleontology*, *51*(2), 101–168. https://doi.org/10.2113/51.2.101

Parsons, T., Wells, R. E., Fisher, M. A., Flueh, E., & Ten Brink, U. S. (1999). Three-dimensional velocity structure of Siletzia and other accreted terranes in the Cascadia forearc of Washington. *Journal of Geophysical Research: Solid Earth*, *104*(B8), 18015–18039. https://doi.org/10.1029/1999jb900106

Personius, S. F., Briggs, R. W., Nelson, A. R., Schermer, E. R., Maharrey, J. Z., Sherrod, B. L., et al. (2014). Holocene earthquakes and right-lateral slip on the left-lateral Darrington–Devils Mountain fault zone, northern Puget Sound, Washington. *Geosphere*, *10*(6), 1482–1500. https://doi.org/10.1130/ges01067.1

Phillips, B. A., Kerr, A. C., Mullen, E. K., & Weis, D. (2017). Oceanic mafic magmatism in the Siletz terrane, NW North America: Fragments of an Eocene oceanic plateau? *Lithos*, *274*, 291–303. https://doi.org/10.1016/j.lithos.2017.01.005

Prothero, D. R., Draus, E., Cockburn, T. C., & Nesbitt, E. A. (2008). Paleomagnetism and counterclockwise tectonic rotation of the upper Oligocene Sooke Formation, southern Vancouver Island, British Columbia. *Canadian Journal of Earth Sciences*, *45*(4), 499–507. https://doi.org/10.1139/e08-012

Regalla, C., Fisher, D. M., Kirby, E., Oakley, D., & Taylor, S. (2017). Slip inversion along inner fore-arc faults, Eastern Tohoku, Japan. *Tectonics*, *36*(11), 2647–2668. https://doi.org/10.1002/2017tc004766

Riller, U., Clark, M., Daxberger, H., Doman, D., Lenauer, I., Plath, S., & Santimano, T. (2017). Fault-slip inversions: Their importance in terms of strain, heterogeneity, and kinematics of brittle deformation. *Journal of Structural Geology*, *101*, 80–95. https://doi.org/10.1016/j.jsg.2017.06.013

Rusmore, M. E., & Cowan, D. S. (1985). Jurassic-Cretaceous rock units along the southern edge of the Wrangellia terrane on Vancouver Island. *Canadian Journal of Earth Sciences*, *22*(8), 1223–1232. https://doi.org/10.1139/e85-124

Sacks, A., Saffer, D. M., & Fisher, D. (2013). Analysis of normal fault populations in the Kumano forearc basin, Nankai Trough, Japan: 2. Principal axes of stress and strain from inversion of fault orientations. *Geochemistry, Geophysics, Geosystems*, *14*(6), 1973–1988. https://doi.org/10.1002/ggge.20118

Schuster, J. E. (2005). *Geologic map of Washington State*. Washington State Department of Natural Resources Olympia.

Sherrod, B. L., Blakely, R. J., Weaver, C. S., Kelsey, H. M., Barnett, E., Liberty, L., et al. (2008). Finding concealed active faults: Extending the southern Whidbey Island fault across the Puget Lowland, Washington. *Journal of Geophysical Research: Solid Earth*, *113*(B5). https://doi.org/10.1029/2007JB005060

Sigloch, K., & Mihalynuk, M. G. (2017). Mantle and geological evidence for a Late Jurassic-Cretaceous suture spanning North America. *GSA Bulletin*, *129*(11–12), 1489–1520.

Snavely, P. D., Niem, A., MacLeod, N., Pearl, J., & Rau, W. (1980). *Makah formation; a deep-marginal-basin sequence of late Eocene and Oligocene age in the northwestern Olympic Peninsula, Washington (Tech. Rep.)*. U.S. Government Publishing Office.

Tiffin, D. L., Cameron, B. E. B., & Murray, J. W. (1972). Tectonics and depositional history of the continental margin off Vancouver Island, British Columbia. *Canadian Journal of Earth Sciences*, *9*(3), 280–296. https://doi.org/10.1139/e72-023

Timpa, S., Gillis, K. M., & Canil, D. (2005). Accretion-related metamorphism of the Metchosin igneous complex, southern Vancouver Island, British Columbia. *Canadian Journal of Earth Sciences*, *42*(8), 1467–1479. https://doi.org/10.1139/e05-043

Vannucchi, P., Maltman, A., Bettelli, G., & Clennell, B. (2003). On the nature of scaly fabric and scaly clay. *Journal of Structural Geology*, *25*(5), 673–688. https://doi.org/10.1016/s0191-8141(02)00066-4

Vannucchi, P., Ranero, C. R., Galeotti, S., Straub, S. M., Scholl, D. W., & McDougall-Ried, K. (2003). Fast rates of subduction erosion along the Costa Rica Pacific margin: Implications for nonsteady rates of crustal recycling at subduction zones. *Journal of Geophysical Research: Solid Earth*, *108*(B11). https://doi.org/10.1029/2002JB002207

Vogt, K., & Gerya, T. V. (2014). From oceanic plateaus to allochthonous terranes: Numerical modeling. *Gondwana Research*, *25*(2), 494–508. https://doi.org/10.1016/j.gr.2012.11.002

Vogt, P. R., Lowrie, A., Bracey, D. R., & Hey, R. (1976). *Subduction of aseismic oceanic ridges: Effects on shape, seismicity, and other characteristics of consuming plate boundaries* (Vol. 172). Geological Society of America. https://doi.org/10.1130/SPE172-p1

Von Huene, R., & Suess, E. (1988). Ocean Drilling Program Leg 112, Peru continental margin: Part 1, tectonic history. *Geology*, *16*(10), 934–938. https://doi.org/10.1130/0091-7613(1988)016<0934:odplpc>2.3.co;2

Wallace, L. M., Ellis, S., & Mann, P. (2009). Collisional model for rapid fore-arc block rotations, arc curvature, and episodic back-arc rifting in subduction settings. *Geochemistry, Geophysics, Geosystems*, *10*(5). https://doi.org/10.1029/2008GC002220

Wang, K., Hu, Y., & He, J. (2012). Deformation cycles of subduction earthquakes in a viscoelastic Earth. *Nature*, *484*(7394), 327. https://doi.org/10.1038/nature11032

Wells, R. E., Bukry, D., Friedman, R., Pyle, D., Duncan, R., Haeussler, P., & Wooden, J. (2014). Geologic history of Siletzia, a large igneous province in the Oregon and Washington Coast Range: Correlation to the geomagnetic polarity time scale and implications for a long-lived Yellowstone hotspot. *Geosphere*, *10*(4), 692–719. https://doi.org/10.1130/ges01018.1

Wells, R. E., Engebretson, D. C., Snavely, P. D., Jr., & Coe, R. S. (1984). Cenozoic plate motions and the volcano-tectonic evolution of western Oregon and Washington. *Tectonics*, *3*(2), 275–294. https://doi.org/10.1029/tc003i002p00275

Yorath, C. J. (1980). The Apollo structure in Tofino basin, Canadian Pacific continental shelf. *Canadian Journal of Earth Sciences*, *17*(6), 758–775. https://doi.org/10.1139/e80-072